Geosystems and Geoenvironment 2 (2023) 100107

Contents lists available at ScienceDirect

Geosystems and Geoenvironment

journal homepage: www.elsevier.com/locate/geogeo

Groundwater potential mapping in hard rock terrain using remote sensing, geospatial and aeromagnetic data

K.S. Ishola[a,*], A.A. Fatoyinbo[a], A.I. Hamid-Mosaku[b], C.J. Okolie[b], O.E. Daramola[b], T.O. Lawal[c]

[a] Department of Geosciences, Faculty of Sciences, University of Lagos, Nigeria
[b] Department of Surveying and Geoinformatics, Faculty of Engineering, University of Lagos, Nigeria
[c] Department of Physics, Faculty of Physical Sciences, University of Ilorin, Nigeria

ARTICLE INFO

Article history:
Received 9 March 2022
Revised 27 May 2022
Accepted 14 July 2022

Editor: E. Shaji

Keywords:
Groundwater
Analytical hierarchical process
Aeromagnetic data
Landsat 8 imagery
Shuttle radar topography mission
Groundwater potential zonation map

ABSTRACT

The need for water security in different regions of the world has led to the deployment of remote sensing (RS) and geographic information systems (GIS) as decision support tools with geophysical methods. In this study, the remote sensing, geospatial and aeromagnetic data were integrated for mapping the groundwater potential at the University of Ilorin, Nigeria in West Africa. Several remote sensing and geospatial datasets (geomorphology, lineament density, slope, rainfall, land use/land cover, soil type and drainage density) were enhanced, weighted, prioritised and ranked using the analytical hierarchy process (AHP) technique. Subsequently, the thematic datasets were integrated into a GIS platform to produce a groundwater potentiality zonation (GWPZ) map. Visualisation of the corrected aeromagnetic data was improved by using some image enhancement techniques (filters) to produce the magnetic anomaly maps that revealed gross and subtle subsurface features. Multiple validation of the GWPZ map was achieved using the magnetic anomalies maps, borehole groundwater potential indices (GWPI) and the receiver operating characteristic (ROC) curves. The GWPZ map generated was classified into three groundwater potential classes with different spatial distributions. These include moderate (60.6%), high (5.9%), and low (33.5%). The magnetic anomalies maps agreed well with the remotely sensed models through surface-subsurface lineaments superposition. The area under curve (AUC) of the ROC showed that the predictive rate of the GWPZ model was 0.73. This value suggested that the model satisfactorily predicted the groundwater potential of the study area. Thus, this present study demonstrated the relevance of geospatial and geophysical techniques for regional groundwater potential mapping at the assessment phase of integrated water resources management towards providing a better understanding of the hydrogeology for easy decision-making and better groundwater management.

1. Introduction

Water is unarguably the most prevalent fluid inside the Earth's crust (Margat and Gun, 2013). Water resources management for sustainable development is of great concern across the globe with about 30% of the total freshwater on the Earth accessible as groundwater (Shiklomanov, 1993; Kalhor et al., 2019). Groundwater is a natural resource of great extent with uneven and boundless availability (Todd, 1980). It is increasingly becoming a vital resource and due to its occurrence, is relatively less vulnerable to contamination than surface-water sources. Tóth (1999) highlighted some of the prioritised criteria for groundwater geo-location and dynamics. These include climate, geology, hydrology, topography, ecology, vegetation, soil distribution, and the formation of the earth's crust through geologic time. The importance of groundwater with respect to the hydrological cycle, plant and soil development, and human activities has been addressed in previous studies. Despite the perceived status of groundwater, its direct observation and traceability has proven to be difficult. Hence, there is a need to adequately monitor and chart the hydrological dynamics of the available groundwater (Levy and Xu, 2011; Coscia et al., 2012).

Groundwater is a prime source of drinking water due to its good quality and low vulnerability to contamination (Li and Qian, 2018; Rao and Chaudhary, 2019). It is the most valuable natural resource in the world, particularly in the arid and semi-arid climo-morphogenetic regions such as the hilly regions of the Himalayas, the tropical Middle East, and the hard rock topogra-

* Corresponding author.
E-mail address: kishola@unilag.edn.ng (K.S. Ishola).

https://doi.org/10.1016/j.geogeo.2022.100107

phy of Africa where subsurface water is only restricted to aquifer pockets within fractured and weathered horizons in the subsurface (Haque et al., 2020). Apart from drinking and public health use, groundwater is used in the sustenance of agriculture, industry, and environmental stability, and has numerous domestic uses. Its urgent need is mostly felt in the Middle East and North Africa where surrogate water resources are inadequate (Sarkar et al., 2020; Karunakalage et al., 2021). As the awareness for water resources management grows, attention is being focused on surface water and groundwater through scientific investigations. In crystalline geological terrain for instance, groundwater moves irregularly due to the variations in subsurface geology and hydrogeological factors thus it is confined to fractured and weathered formations (Adiat et al., 2012; Machiwal and Jha, 2014; Ejepu et al., 2017). This irregularity might be responsible for the failure or low success rate in borehole drilling in these hydro-geologically complex regions within which our study area in North-central Nigeria is located.

In delineating groundwater zones on a regional scale, the sole reliance on conventional techniques of borehole pumping tests and/or the use of point-scale geophysical techniques such as the one-dimensional (1D) Vertical Electrical Sounding (VES) in estimating aquifer characteristics for groundwater productivity potential is insufficient particularly in this era of fast decision-making. Hence, integrating remote sensing and geospatial data, and traditional geophysical techniques gives a better understanding of physical factors affecting the hydrogeology (Grauch and Bankey, 2003; Haque et al., 2020). Globally, groundwater is adjudged to be the next scarcest resource, especially in the face of exponential population growth, climatic variability, and rising abstraction from agricultural and industrial uses (Ahner, 2013; Anuforum, 2013). According to resource experts, groundwater management will be an enduring gauge in water and land management (Foster et al., 2006a; Jha et al., 2007; Majumder, 2015). Since major portions of our ecosystem are largely water-dependent and freshwater is a germane ingredient to our ecosystem's stability and sustainability, groundwater research is a national and global concern (Foster et al., 2006b).

The traditional drilling test is one of the many techniques available for siting boreholes and evaluating the thickness of aquiferous units (Madan et al., 2010; Adiat et al., 2012). However, it is limited in use due to time, cost, as well as being point specific (Arisona et al., 2020). The application of geospatial techniques has overcome these pitfalls by providing a time-effective coverage of attributes that may reveal regional surficial geologies and structures that could aid in the effective assessment of groundwater resources (Greenbaum, 1992; Hoffmann and Sander, 2007; Jha et al., 2007). Satellite remote sensing provides satellite imageries which can also be used for reconnaissance surveys (Prasad et al., 2008). Elsewhere, satellite imageries have been very effective in the extraction of geomorphological and hydrological units for groundwater prospects mapping (Agarwal and Garg, 2016). Due to the spatio-temporal variation of groundwater potential, its study requires a consideration of various spatial and environmental factors which are of hydro-geological significance.

In the Sub-Saharan Africa region, the hard rock terrain also known as the crystalline basement covers about forty percent of the 23.6 million square kilometres of landmass while other hydrostratigraphic units (including the volcanic rocks of East Africa) occupy the rest of the province (MacDonald et al., 2008). This means that the crystalline basement and volcanic rocks are the two major hydro-geological provinces in Africa where groundwater exploration follows no standard rule of thumb and requires in-depth investigation. Such a situation can be cumbersome and requires sophisticated technologies (Foster et al., 2006a; MacDonald et al., 2008). Furthermore, in hard rock terrain, water is found in pockets at depths and often in unconnected fractures and faults, and an integrated approach toward groundwater development has been advocated for (WMO, 2012; IGRAC, 2018). The integrated water resources management (IWRM) approach aids decision-making in groundwater resources development by prospecting for and managing groundwater resources in three phases: assessment, development, and monitoring (WMO, 2012).

It is evident from the extant literature that a lot of work has been carried out on the application of geospatial technology (i.e., remote sensing and GIS) in groundwater exploration. Geospatial tools have become pervasive in water resources management, especially in developing nations (Kumar et al., 2010; Ejepu et al., 2015, 2017; Amadi and Olasehinde, 2010; Anifowose and Aladejana, 2015; Jesiya and Gopinath, 2019). In the works of Fashae et al. (2013) and Akinlalu et al. (2017), geospatial techniques were used for the quantification of groundwater potential zones in crystalline basements of south-western Nigeria. In the alluvial environment of south-east Asia, an integrated study using RS/GIS for groundwater potentiality mapping was carried out and a prediction map that was about 81.3% in agreement with the ground truth data was produced (Adiat et al., 2012). Elsewhere, Ranganai and Ebinger (2008), Elbeih (2015) and Muthamilsevan et al. (2017) delineated and identified structures that aided regional groundwater exploration through the integration of aeromagnetic data, remote sensing and GIS techniques in Zimbabwe Craton, North Africa and India.

Geophysical methods have been used in addressing several hydro-geological problems (Mazac et al., 1987; Adiat et al., 2013; Mogaji, 2016). The use of geophysics for groundwater resource mapping is driven by the desire to reduce the risk of drilling non-productive boreholes as well as to avert the huge costs associated with low groundwater availability. Aeromagnetic survey is a conventional geophysical prospecting method in which the geomagnetic field of the Earth is measured with a magnetometer mounted on an aircraft (Kearey and Brooks, 1991). In regional studies, aeromagnetic surveys have been used in surface geologic mapping where the magnetic effects of geologic features such as basement faulting system that represents fluid paths are delineated (Grauch and Bankey, 2003; Ndikilar et al., 2019). It has also been applied in the mapping of bedrock architecture (Okpoli and Oladunjoye, 2017; Zhou, 2018) and groundwater reservoirs in hard rock terrain (Ranganai and Ebinger, 2008). Despite their potentials, aeromagnetic surveys have not been adequately explored in previous studies for groundwater potential zonation, particularly in the North-central basement complex of Nigeria. Within this region, the University of Ilorin (UNILORIN) and its environs in the Ilorin South local government area (LGA) are situated.

To the best of our knowledge, this study was the first to integrate remote sensing, geospatial data, and geophysical technique for a quasi-regional groundwater zonation to aid decision-making and water management in Ilorin. Also, an effort to update the methodology and advance the frontier knowledge based on groundwater sustainability delineation through a remote sensing and GIS-based operationalisation of robust criteria identified through reviewed literature and a multi-criteria decision-based analytical hierarchy process was undertaken (Jasrotia et al., 2013, 2016, 2019; Khan et al., 2020). Since the sustainable use of groundwater depends on its availability, storability and usability, another objective of this study was to produce a groundwater prospective zones model within Ilorin South LGA with a focus on UNILORIN landmass. Furthermore, this study adopted a multi-level approach for validation of the groundwater potential map generated towards ensuring a long-time plan for sustainable groundwater management. Thus, the principal objective of our study was to characterise the spatial distribution of groundwater potential in our region of

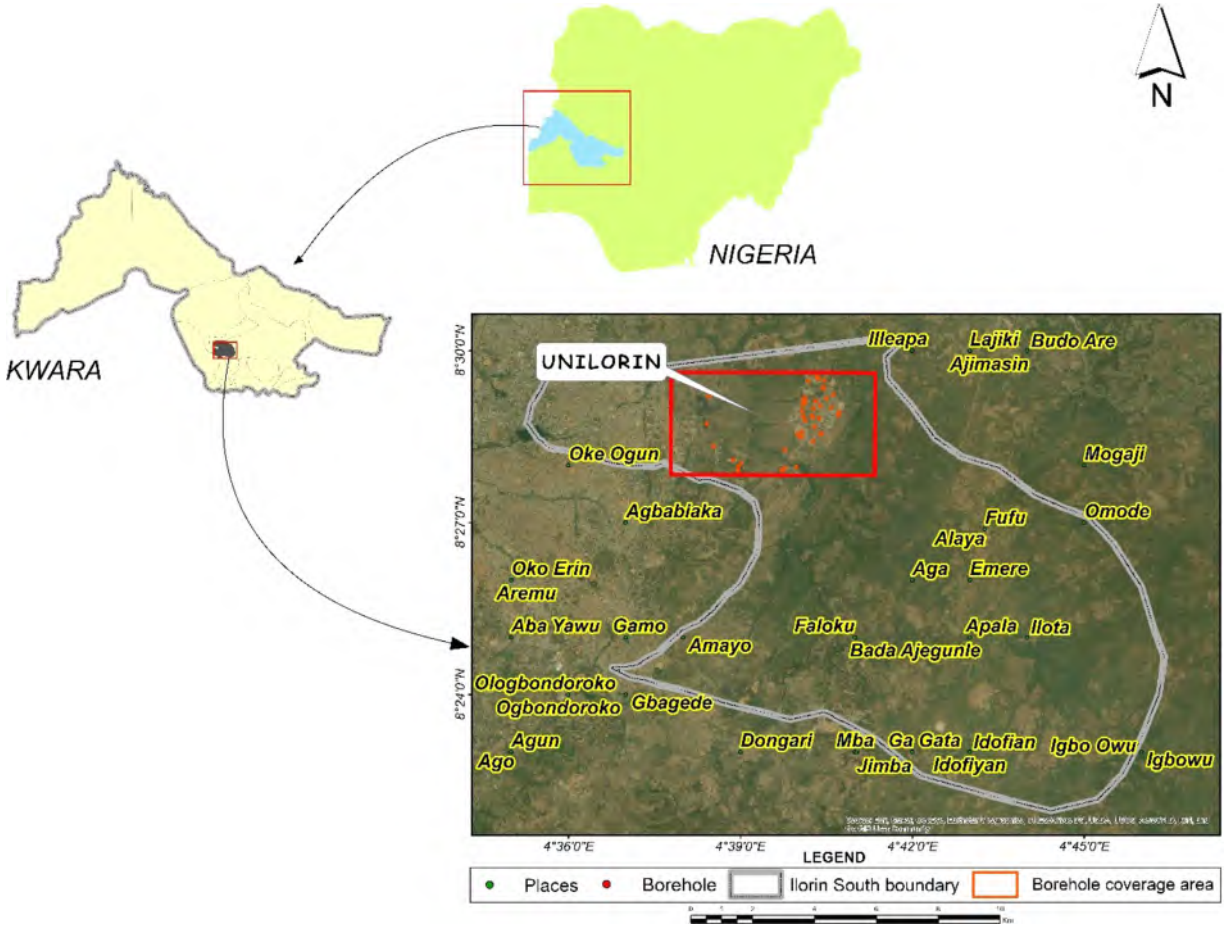

Fig. 1. The map of Nigeria and study area. The zoomed image of the study area (UNILORIN) and the adjoining areas on a high-resolution Digital Terrain Model is also shown.

interest through the integration of geospatial and geophysical analysis.

2. Location, geomorphology and geology of the study area

The study area is the University of Ilorin (UNILORIN) landmass in Ilorin South Local Government Area of Kwara State, North-central Nigeria shown in Fig. 1. It is about 15 km from the main township with an areal extent of about 15,000 hectares (150 km^2). Geographically, it is located between Longitudes 4°39′ E-4°42′ E and Latitudes 8°27′ N-8°29′ N. This geographic extent encompasses built-up areas which are the most anthropogenically active zones within the landmass.

The three major constituents of the geology of Nigeria are the Crystalline Basement Complex, the Jurassic Granites, and Cretaceous-to-Quarternary Sedimentary Sequences (Okunlola, 2012; MMSD, 2017). The Basement Complex covers more than half of Nigeria's subsurface. The Precambrian and Phanerozoic rocks in the Eastern and North-central regions of Nigeria are the major constituents of the basement complex. The Precambrian basement complex is characterised by three major lithologic successions which are: undifferentiated Migmatite-Gneiss-Quartzite complex of Archaen to early Proterozoic origin (2700-2000 Ma), Metavolcanic-sedimentary rocks of late Proterozoic age (c. 5420 Ma), and the Older granite complex of Late Precambrian to lower Paleozoic age (5420-2510 Ma) also known as Pan-African granites all of which were affected by the Pan-African orogeny (Oyawoye, 1972; Black et al., 1979; Ajibade et al., 1987; Rahaman, 1988; Caby, 1989; Dada, 2008; all cited in Omeje et al., 2014; MMSD, 2017). The basement rock with low transmittivity of about 31 m^2/day inherently does not make a good aquifer (FMWR, 2014). The sedimentary sequences which are vast depressions between basement landmasses and the Younger granites filled up the basins with the creation of some basins. The Bida Basin of the Benue Trough which is synonymous with the geology of North-central Nigeria (MMSD, 2017) is one of the basins.

Geologically, UNILORIN is underlain by rocks of crystalline basement complex together with the granite suite (foliated granodiorite, foliated microgranites as well as older granites). Others are the gneiss complex (augen gneiss, banded gneiss and granite gneiss) and the veins (pegmatite and quartz veins) (Olasehinde and Raji, 2007; Raji and Bale, 2008). These crystalline rocks are emplaced in Precambrian times, and are usually the major targets during any geophysical survey (Olasehinde, 1984; Adelana, 1988; Nwankwo, 2002; Nwankwo, 2011; Lawal et al., 2012). Although the basement complex dominated the area, processes such as the increase in temperature, pressure, and chemical changes resulted in metamorphism leading to the formation of sedimentary rocks. Furthermore, the surficial layer consists of laterites, clayey soil and alluvial deposits (Jimoh, 1997; Raji and Bale, 2008). These types of deposits are weak and readily yield to agents of erosion (Jimoh, 1997). Some visible exposures of the bedrock in the adjoining areas such as Amoyo and Ganmo are evident (Olawepo et al., 2013).

3. Materials and methods

A workflow diagram of the procedure for the data acquisition, data processing, and analysis is shown in Fig. 2. These stages are discussed in the following sections.

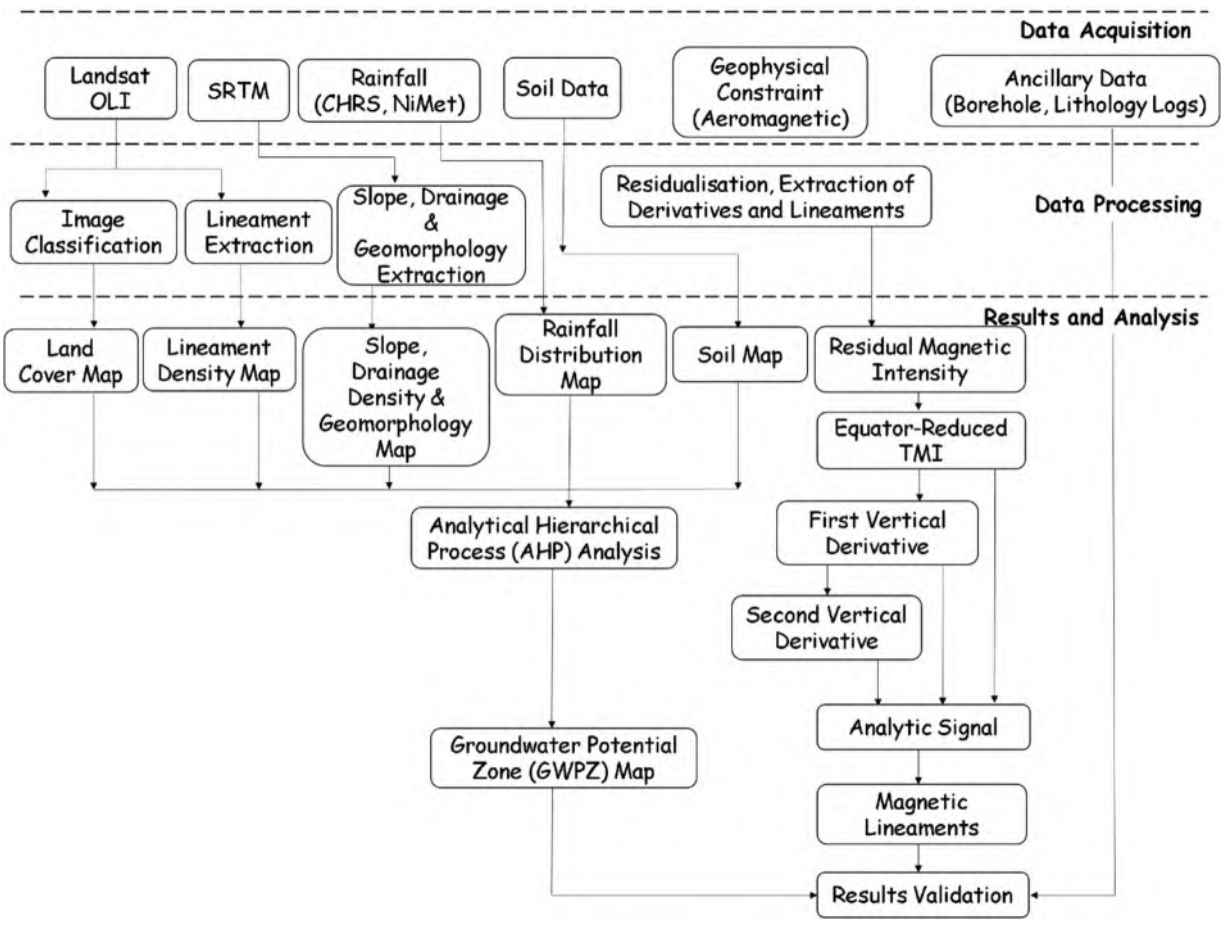

Fig. 2. A workflow diagram of the methodology showing the various stages used to generate the groundwater potential zonation map for the study area.

3.1. Data acquisition and preparation of thematic layers

In this study, Landsat 8 Operational Land Imager (OLI) imagery (acquisition date: 31 March, 2019), 3 arc-second/30-metre resolution Shuttle Radar Topography Mission digital elevation model (SRTM DEM) version 3.0 (acquisition date: February, 2000) and aeromagnetic data of Ilorin (Sheet 223) were used. The Landsat imagery and SRTM DEM were acquired from the United States Geological Surveys, USGS (USGS, 2013; 2020; https://earthexplorer.usgs.gov/) web portal. The use of multi-spectral Landsat imagery enabled the classification of land use/land cover (LULC; Nse et al., 2020). Also, satellite-derived DEMs such as SRTM have found wide applications in terrain modelling, earthworks, geomorphological modelling, urban planning and engineering (Nwilo et al., 2020). Aeromagnetic data was obtained from the Nigeria Geological Survey Agency (NGSA, 2010; https://ngsa.gov.ng/). Other datasets include climatic (rainfall) data from the Nigerian Meteorological Agency (NiMet, 2010) and Centre for Hydrometeorology and Remote Sensing (CHRS, 2019), soil data from the Federal Department of Agricultural Land Resources (FDALR, 1990), borehole inventory and lithologs. The PERSIANN-CDR (Precipitation Estimation from Remote Sensing Information using Artificial Neural Network-Climate Data Record) rainfall data from CHRS is a quasi-real-time satellite hydro-meteorological dataset. Most data recorded in terrestrial weather observatories such as those operated by NiMet usually fulfil temporal variability requirements, but their deficit is in spatial coverage. Hence, in recent times, quasi real-time satellite hydro-meteorological data such as PERSIANN-CDR have been used (either as reinforcement or standalone data) to constrain and augment the deficits in data from terrestrial observatories (Nguyen et al., 2019). This augmentation is necessary since comprehensive climate data are expected to fulfil the requirements of spatial coverage and temporal variability (WMO, 2012; Nguyen et al., 2019). Table 1 shows the characteristics of the datasets.

3.2. Data pre-processing and image enhancement

The datasets were harmonised and projected onto a common Universal Transverse Mercator (UTM) coordinate system (WGS84 Zone 31N) in order to avoid errors in the linear measurement, and to preserve the geometric properties of the datasets. The thematic layers were re-sampled using the nearest neighbour resampling method and resized to 30 m for conformity with the spatial resolution of the Landsat imagery. The Landsat imagery was enhanced in ENVI software v5.3 environment by the generation of a false colour composite using three spectral bands in the order – band 6 (Shortwave Infrared), band 5 (Near Infrared) and band 4 (Red).

3.3. Data processing

Data processing entailed the land use/land cover (LULC) extraction, lineaments extraction, generation of rainfall, slope and drainage density maps, extraction of soil and geomorphology, and production of maps for the total magnetic intensity (TMI) and its derivatives. Also, the Groundwater Potential Zonation (GWPZ) map was produced from the aforementioned layers using a multi-criteria decision-making technique known as the analytical hierarchy process (AHP) implemented via weighted overlay. The key

Table 1
Information and characteristics of datasets used in this study.

Data	Source	Scale/ Resolution	Epoch	End Product
Landsat 8 imagery path 190, row 054	USGS	30m	31st March, 2019	Land cover map, Lineaments Density map
SRTM DEM (version 3.0)			2000	Drainage Density map, Slope map
Soil vector layer	FDALR	-	1990	Geomorphology map
		-		Soil map
Aeromagnetic data	NGSA (Sheet 223)	High Resolution Aeromagnetic Data (HRAM)	80m Mean Terrain Clearance (MTC) Acquired 2006	Derivatives and lineaments
Climatic data (Annual rainfall)	NiMet and CHRS	PERSIANN 0.25° × 0.25°	Static and PERSIANN-CDR 18 years (2001 – 2018)	Rainfall map
Borehole inventory	UNILORIN Works Department (UWD)	47 Boreholes		GWPZ (Validation)
Lithology logs	UWD/Phillip Morris /Journals			Lithology and depth

stages of the preparation of the GWPZ map are discussed in the sections that follow.

3.3.1. Land use/land cover (LULC) extraction

The following LULC classes were identified through interpretation of the Landsat image composite in line with Anderson's Level I classification scheme (Anderson et al., 1976) for remotely sensed data: built-up area, water body, forest land and agricultural land. To extract LULC classes, the composite was subjected to supervised image classification using the maximum likelihood classification (MLC) technique. The MLC algorithm uses a statistical approach for pattern recognition and makes assumptions that the statistics of each class in the image band are normally distributed (Harris Geospatial, 2020). The MLC algorithm computed the likelihood of any given pixel that belongs to each class, then assigned it to a class (Hasmadi et al., 2009; Ahmad and Quegan, 2012; Huang et al., 2015; Nse et al., 2020). MLC is simple to implement and is widely used for various remote sensing applications (Lillesand et al., 2000; Otukei and Blaschke, 2010; Ahmad and Quegan, 2012; Nse et al., 2020). The overall accuracy of the classification was also assessed. Accuracy assessment is important for checking the quality of results and has been used extensively in LULC studies (Ishola et al., 2014; Alademomi et al., 2020; Nse et al., 2020). The classification output was compared with the Landsat imagery at fifty-four (54) coincident points. This comparison enabled the detection of omission errors (pixels belonging to one class but included in other classes), commission errors (pixels assigned to a certain class that did not belong to it), and correctly classified pixels (Ishola et al., 2014). The overall accuracy was then computed using Eq. 1.

$$Overall\ accuracy\ (\%) = \frac{Total\ number\ of\ correct\ samples}{Total\ number\ of\ samples} \times\ 100 \quad (1)$$

The output of the classification was exported to ArcGIS to cross-check the classification results and for editing.

3.3.2. Lineament extraction

A directional convolution filter with a 5 × 5 kernel size was applied to the Landsat image composite to improve its spatial frequency. This enhancement was done within the ENVI software environment. Following the approach of Epuh et al. (2020), the filter was applied in the four principal directional angles of N-S (180°), NW-SE (135°), NE-SW (225°) and E-W (270°). The output of the convolution was four sets of spatially filtered images with enhanced brightness values. The filtered images were then imported into the PCI Geomatica (version 2018) environment. To extract the lineaments, edge-detection, thresholding and curve extraction were executed using the Line module. The implementation of the Line module was based on parameters that defined the numbers and lengths of extracted lineaments. A description of these parameters is provided in Hubbard et al. (2012), El-Sawy et al. (2016) and Epuh et al. (2020). The extracted lineaments were converted to ESRI shapefile format and further processed with the Line density tool in the ArcGIS spatial analyst extension to yield a lineament density map.

3.3.3. Generation of slope map

The slope tool in the ArcGIS 3D Analyst was used to generate a slope map (in degrees) from the SRTM DEM. The slope function identifies the gradient, or rate of maximum change in z-value from each cell of the DEM, with a range from 0° to 90°. The slope tool was used to calculate the maximum rate of change of a particular cell to its neighbouring cells. The maximum change in elevation over the distance between the cell and its eight neighbouring cells identified the steepest downhill descent from the cell.

3.3.4. Generation of other thematic layers

The PERSIANN rainfall data was interpolated to a raster surface of 30 m spatial resolution using kriging interpolation. Although the NiMet data was not adequate to serve as the primary rainfall dataset, it was used to validate the PERSIANN data through a Pearson's correlation analysis (2-tailed) at the 0.05 significance level. This was done to confirm that both datasets exhibited a similar trend. The soil layer was clipped out from the digitised soil map and converted to raster format using the polygon-to-raster tool in ArcGIS. The geomorphology map was generated through a reclassification of the SRTM DEM while the drainage density map was generated by running the line density function on drainage channels extracted from the DEM.

3.3.5. Weighting and overlay of the thematic layers

The thematic layers were assigned weights using the analytic hierarchy process (AHP) method developed by Saaty (1980). The AHP is a well-structured tool for managing both qualitative and quantitative multi-criteria elements for decision-making. It makes judgments and calculations easy because of pairwise comparison of matrices of the identified criteria (i.e., the thematic layers, as in this study). Moreover, it demonstrates the compatibility and incompatibility of decisions which is the recompense of multi-criteria decision-making (Lee, 2007). The principle of AHP is well documented in the literature (e.g., Saaty, 1988; Adiat et al., 2012; Adiat et al., 2013; Hamid-Mosaku, 2014; Brunelli, 2015; Hamid-Mosaku et al., 2016; Reisi et al., 2018; Hamid-Mosaku et al., 2020). In the initial criteria selection, 12 thematic layers were identified: drainage density, lineament density, LULC, soil, annual rainfall, slope, magnetic intensity, geomorphology, roughness, geology,

Table 2
Pairwise comparison matrix, $\breve{D}$ of the criteria.

Layer	Dd	Ld	LC	SC	AR	S	MI	Gm	R	Gl	TWI	TPI
Dd	1	3	3	3	3	3	4	4	4	5	5	6
Ld	0.33	1	3	3	3	3	4	4	4	5	5	6
LC	0.33	0.33	1	3	3	3	5	4	4	5	5	6
SC	0.33	0.33	0.33	1	3	3	4	4	4	5	5	6
AR	0.33	0.33	0.33	0.33	1	3	3	3	3	4	5	5
S	0.33	0.33	0.33	0.33	0.33	1	3	3	3	4	4	5
MI	0.25	0.25	0.2	0.25	0.33	0.33	1	3	3	3	4	4
Gm	0.25	0.25	0.25	0.25	0.33	0.33	0.33	1	3	3	3	3
R	0.25	0.25	0.25	0.25	0.33	0.33	0.33	0.33	1	3	3	3
Gl	0.20	0.20	0.20	0.20	0.25	0.25	0.33	0.33	0.33	1	3	3
TWI	0.20	0.20	0.20	0.20	0.2	0.25	0.25	0.33	0.33	0.33	1	3
TPI	0.17	0.17	0.17	0.17	0.2	0.2	0.25	0.33	0.33	0.33	0.33	1

Dd: Drainage density; Ld: Lineament density; LC: Land cover; SC: Soil class; AR: Annual rainfall; S: Slope; MI: Magnetic intensity; Gm: Geomorphology; R: Roughness; Gl: Geology; TWI: Topographic wetness index; TPI: Topographic position index

Table 3
Normalised comparison matrix (R). Table 3 Normalised comparison matrix (R).

Layer	Dd	Ld	LC	SC	AR	S	MI	Gm	R	GI	TWI	TPI
Dd	0.2510	0.4511	0.3237	0.2503	0.2002	0.1695	0.1569	0.1463	0.1333	0.1293	0.1154	0.1176
Ld	0.0837	0.1504	0.3237	0.2503	0.2002	0.1695	0.1569	0.1463	0.1333	0.1293	0.1154	0.1176
LC	0.0837	0.0501	0.1079	0.2503	0.2002	0.1695	0.1961	0.1463	0.1333	0.1293	0.1154	0.1176
SC	0.0837	0.0501	0.0360	0.0834	0.2002	0.1695	0.1569	0.1463	0.1333	0.1293	0.1154	0.1176
AR	0.0837	0.0501	0.0360	0.0278	0.0667	0.1695	0.1176	0.1098	0.1000	0.1034	0.1154	0.0980
S	0.0837	0.0501	0.0360	0.0278	0.0222	0.0565	0.1176	0.1098	0.1000	0.1034	0.0923	0.0980
MI	0.0628	0.0376	0.0216	0.0209	0.0222	0.0188	0.0392	0.1098	0.1000	0.0776	0.0923	0.0784
Gm	0.0628	0.0376	0.0270	0.0209	0.0222	0.0188	0.0131	0.0366	0.1000	0.0776	0.0692	0.0588
R	0.0628	0.0376	0.0270	0.0209	0.0222	0.0188	0.0131	0.0122	0.0333	0.0776	0.0692	0.0588
Gl	0.0502	0.0301	0.0216	0.0167	0.0167	0.0141	0.0131	0.0122	0.0111	0.0259	0.0692	0.0588
TWI	0.0502	0.0301	0.0216	0.0167	0.0133	0.0141	0.0098	0.0122	0.0111	0.0086	0.0231	0.0588
TPI	0.0418	0.0251	0.0180	0.0139	0.0133	0.0113	0.0098	0.0122	0.0111	0.0086	0.0077	0.0196
Consistency Index (CI) = 0.1429; Random Index (RI) =1.48; Consistency Ratio (CR) = 0.0966												

topographic wetness index, and topographic position index. However, only seven of the thematic layers were retained in the final selection based on the ranking and data availability. The data on magnetic intensity was retained as an auxiliary layer for the groundwater analysis and validation. To guide the weighting, an online questionnaire was prepared and distributed to groundwater management experts, some of whom were knowledgeable about the study area, and ten responses were received. Their responses were averaged and a pairwise comparison was carried out based on the AHP model. According to Hamid-Mosaku et al. (2017), pairwise comparison matrices (D) of decisions take the form shown in Eq. 2 where the elements $\{x_{ij}\}$ of the matrix is the degree of preference of the ith criterion over the jth criterion or vice versa for the determination of the relative priorities of all the criteria.

$$D_{ij} = \left(x_{ij}\right) \tag{2}$$

In aggregating the responses from the experts, the average pair wise comparison matrix ($\breve{D}$) was determined using Eq. 3 and the results are shown in Table 2.

$$\breve{D}_{ij} = \left(\breve{x}_{ij}\right) \tag{3}$$

The normalized comparison matrix (R) was computed using Eq. 4. The results are shown in Table 3. The priority weights of individual layers shown in Table 4 were obtained from the normalized comparison weights.

$$R_{ij} = \frac{x_{ij}}{\sum_{i=1}^{n} x_{ij}} \tag{4}$$

The consistency index (CI) was computed using Eq. 5 while the consistency ratio (CR) was estimated using Eq. 6 according to Hamid-Mosaku et al. (2017). The random index value which is a direct function of the number of criteria considered was obtained from a lookup table of random indices according to Saaty and Kearns (1985). The CR value being less than 0.1 shows the acceptability of both the survey and the experts' judgement.

Table 4
Priority weights of all 12 thematic layers.

Layer	Priority weight
Drainage density	0.2037
Lineament density	0.1647
Land Cover	0.1417
Soil Class	0.1185
Annual Rainfall	0.0898
Slope	0.0748
Magnetic Intensity	0.0568
Geomorphology	0.0454
Roughness	0.0378
Geology	0.0283
Topographic Wetness Index	0.0225
Topographic Position Index	0.0160

$$CI = \frac{\lambda_{max} - n}{n - 1} \tag{5}$$

where λ_{max} represents the principal eigenvalue of the matrix D having an order of n which is the number of criteria considered.

$$CR = \frac{CI}{RI} \tag{6}$$

The weights derived for the layers and the ranks of the subclasses were inputted into the weighted overlay tool within the ArcGIS environment. The output of the weighted overlay process was reclassified into three classes namely: high, moderate, and low groundwater potential.

The final seven (7) selected thematic layers were integrated using the groundwater potential index (GWPI) in Eq. 7 (Fashae et al., 2013). The GWPI was estimated from the integration of the total normalized weights for the layers. Eq. 7 was implemented using the raster calculator tool in the ArcGIS 10.4 environment after which the overall groundwater potential map was produced. The groundwater potential zones (GWPZ) map was prepared by integrating the information from the aforementioned layers in the ArcGIS environment.

$$GWPI = Dd_w Dd_{w_i} + Ld_w Ld_{w_i} + LULC_w LULC_{w_i} + SC_w SC_{w_i} + AR_w AR_{w_i} + S_w S_{w_i} + Gm_w Gm_{w_i} \quad (7)$$

where, *Dd* is drainage density, *Ld* is lineament density, *LULC* is land use/land cover, *SC* is soil class, *AR* is annual rainfall, *S* is slope, *Gm* is geomorphology, *w* is normalized weight of the thematic layer and w_i is the normalized weight of sub-layer classes.

3.3.6. Processing of magnetic data

Data processing was carried out using a data processing and analysis program known as Oasis Montaj™ software (Geosoft, 1997). To interpret the aeromagnetic anomalies associated with the study area, filters were applied to the magnetic data (i.e., raw total magnetic intensity) to enhance some characteristics of the magnetic sources. This was done using fast fourier transformation (FFT) in the frequency mode. The image enhancement techniques used to suppress or enhance certain magnetic anomalies during the interpretation process include: the reduction to equator (RTE), first and second vertical derivatives (FVD and SVD), and analytic signal (AS). For this study, the maps of the aforementioned data enhancement routines were generated in the Oasis Montaj environment using MAGMAP GX. A brief description of the concept, formulation, and applications of some of these enhancement techniques is discussed below.

3.3.6.1. Total magnetic intensity. The aeromagnetic data was subjected to first-order residualisation in order to generate the total magnetic intensity (TMI) after removal of geomagnetic gradient using the International Geomagnetic Reference Field (IGRF) epoch 2005. This was done to eliminate the effect of deep-seated sources (regional) on the residual magnetic intensity (RMI). Some image enhancement filters were applied to the RMI image to aid visualization and interpretation. Image enhancement is necessary so that subtle magnetic signatures especially those related to edge detection and lithological contrasts are identified (Ranganai and Ebinger, 2008).

3.3.6.2. Reduction to equator. Reduction to the equator (RTE) is required to filter the magnetic data so that the peaks and gradients of magnetic anomaly are directly below their magnetic sources and for better interpretation. RTE removes asymmetries associated with low magnetic latitude anomalies (Balogun, 2019). A rapid change in the subsurface geologic conditions and/or lithologic characters could be achieved through a simple approach of visual inspection of RTE to improve the realistic estimates of the source locations.

3.3.6.3. First and second vertical derivatives. The First vertical derivative (FVD) is one of the derivatives that have been used to emphasize the edges of magnetisation boundaries especially in mapping contacts, faults, dykes, and ore bodies. The FVD enhances the high frequency component of magnetic fields and suppresses the low frequency content due to the regional field using a fast fourier transform (Paine, 1986). An FVD enhancement filter was applied to the RTE data obtained from the gridded TMI data to emphasize the near-surface geological features. The first vertical derivative is given in Eq. 8 as:

$$FVD = \frac{\partial M}{\partial Z} \quad (8)$$

where M is the observed magnetic field.

The Second vertical derivative (SVD) is the second-order derivative of the FVD. The SVD helps in further enhancing the magnetisation boundaries though it is prone to cultural noise and artefacts (Skiba et al., 2016; Ozebo et al., 2017). The enhancement of boundaries of anomalous sources can be performed using the SVD.

3.3.6.4. Analytic signal. An Analytic signal (AS) filter was used to enhance near-surface features and produce maxima directly over magnetic sources, thus making shallow sources more dominant (Skiba et al., 2016). In comparison with FVD, the AS reveals more details of the short-wavelength anomalies, and structures that have been revealed in FVD can be traced more precisely from AS. Thus, the AS is best used for identifying contact locations (Abu El-Ata et al., 2013; Ibraheem et al., 2019). The amplitude of AS can be computed from the first-order horizontal and vertical derivatives of the observed magnetic anomaly or directly from RTE and FVD (Srivastava and Agarwal, 2010; Skiba et al., 2016). Source magnetic anomalies are naturally asymmetrical due to the source magnetisation (source polarization vector) and the earth's magnetic field directions (Srivastava and Agarwal, 2010). Thus, AS uses the Hilbert transform to determine the geometry of magnetic sources. The amplitude of AS also called the total gradient is the square root of the sum of squares of the derivatives in the *x, y* and *z* directions and is expressed in 3D according to Roest et al. (1992) in Eq. 9.

$$|AS(x,y)| = \sqrt{\left(\frac{\partial M}{\partial x}\right)^2 + \left(\frac{\partial M}{\partial y}\right)^2 + \left(\frac{\partial M}{\partial z}\right)^2} \quad (9)$$

where M is the observed magnetic field at (*x, y*) and $\frac{\partial M}{\partial z}$ is the first-order derivative of the observed field.

3.4. Validation of the groundwater potential model

The groundwater potential map was validated with well/borehole location data using the receiver operating characteristic (ROC) technique. According to Zhang et al. (2015), ROC curves can discriminate between observed and predicted variables based on the logistic regression S-shaped curve. The ROC curve technique follows a binary classification rule resulting in four possible consequences: true positive, true negative, false positive, and false negative. A true positive occurs when a correct result is identified correctly as being positive, while a false positive identifies a negative result as being incorrectly a positive. On the other hand, a true negative occurs when a negative result is identified correctly as being negative, while a false negative identifies incorrectly a true result as being negative (Carter et al., 2016). ROC curves were obtained by plotting the true positive rate (sensitivity) on the ordinate against the false-positive rate (1-specificity) on the abscissa while the area under curve (AUC) is the accuracy of the predicted plots. The sensitivity is the proportion of positives that are correctly identified also known as the true-positive rate (Eq. 10), while the specificity is defined as the proportion of negatives that are identified correctly, also known as the true-negative rate. The false-positive rate (1-specificity) is the proportion of incorrect positive results that are negative (Eq. 11). The false-negative rate (1-sensitivity) is the proportion of incorrect results that are positive (Nelson et al., 2005). The ROC curve tool in the statistical package for the social sciences (SPSS) software environment was used to generate the ROC curve.

$$\text{True positive rate} = \frac{\text{True positives}}{\text{True positives} + \text{False negatives}} \quad (10)$$

$$\text{False positive rate} = \frac{\text{False positives}}{\text{True negatives} + \text{False positives}} \quad (11)$$

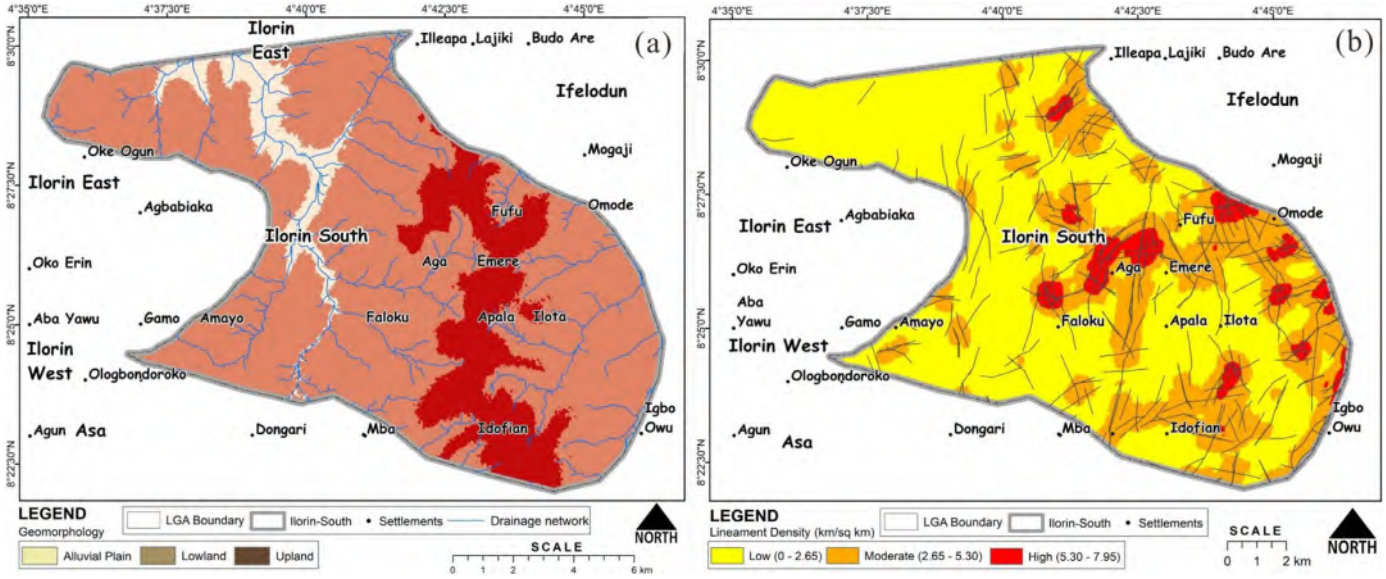

Fig. 3. (a) Geomorphology map suggests that the area is categorised into three classes: the alluvial plains, lowlands and uplands. The alluvial plain resulted from the assemblage of sediments from River Oyun. The lowlands aid rainwater and irrigation water retention while the uplands reflect the secondary porosity that governs the percolation of precipitation into the subsurface, and (b) lineament density map plays significant role in the groundwater storage of the study area. The lineament density gives the concentration of lineaments and it is categorized into three classes: low (0-2.65) dominant; moderate (2.65-5.30); high (5.30-7.95).

The accuracy of the GWPI values obtained was determined in relation to the status of the borehole details. The functional boreholes are the productive boreholes while the dysfunctional/non-functional boreholes are the non-productive boreholes. According to the ROC curve/model, the dependent variable also known as the state variable is a binary data type while the independent variable known as the test variable can be categorical or continuous. For the validation of the GWPI map, the borehole status field was used as the state variable where the functional status was represented with 1 and the dysfunctional 0, while the GWPI field was used as the test variable.

4. Results and analysis

4.1. Analysis of thematic layers and their influences

The maps generated for the seven thematic layers are shown in Figs. 3-6. The importance of each thematic layer with respect to groundwater recharge, runoff, occurrence and storage is discussed below. According to Swetha et al. (2017), parameters for identifying groundwater prospects are almost infinite depending on regional peculiarities. However, geomorphology, slope, drainage density, lineament density, soil, rainfall and land use/land cover are among the most widely adopted.

4.1.1. Geomorphology

In terms of geomorphology, the area is categorised into alluvial plains, lowlands and uplands respectively as shown in Fig. 3a. Permeability can be deduced from the lithology, structure of rocks and unconsolidated deposits. The grain size of rock materials relates to the primary porosity while structures and erosional features such as karsts, lowlands and uplands define the secondary porosity which aids the percolation of precipitation into the subsurface. For the map of Ilorin South as depicted in Fig. 3a, the long perch of alluvial plain is suspected to be an assemblage of sediments from River Oyun, the main source of the university dam which is along the path of the flood plain. The alluvial plain which forms a low gradient of fluvial landforms would help to retain precipitation water in the area. The lowlands could also aid rainwater and irrigation water retention. Overall, the geomorphology of the area has a positive impact on water recharge and storage.

4.1.2. Lineament density

Lineaments are mainly associated with faults or fractures, and are also suggestive of subsurface structures such as lithological boundaries, contacts between land use and drainage lines (Sander, 2007). Lineaments are significant in groundwater potentiality mapping since they are linear features that serve as channels or conduits for groundwater movement and accumulation. In Fig. 3b, high lineament density is observed in the north-central and north-eastern parts while low lineament density dominated the north-western and southern parts of the study area. From this map, we can get qualitative hints that the anthropogenically active zones of UNILORIN landmass (NNW) have low surface lineaments and consequently less subsurface fracturing. Generally, the UNILORIN area has low lineaments density and this would imply that subsurface features (i.e., fissures, joints, fractures) that could serve as groundwater repositories do not exist in that area. Moreover, this could also suggest little or no seismic/tectonic activity occurrences in the area. With respect to groundwater storage potential, the areas around the UNILORIN active area (NNW) have the least storage capacity. Consequently, it is suspected that the local aquifer systems within UNILORIN are not being actively recharged, thus signalling that the main source of groundwater is most likely fossil water. Another possibility could be the presence of large interconnected fractures and a good pressure gradient that would aid the migration of groundwater from the high lineament zones of the central area and SE to the NW.

4.1.3. Slope

The slope map is shown in Fig. 4a. The degree of slope determines whether the zone can retain water by infiltration or encourages runoff (Magesh et al., 2012). Topographic data are very important in water resources assessment (WRA) because they give an overview of the shape, relief and infrastructure of the studied area. Thus, they are essential in understanding the direction of flow and movement of water through catchments to qualify and/or quantify an aquifer's rate of recharge or discharge. Topography is also important in water quality studies to identify potential zones of

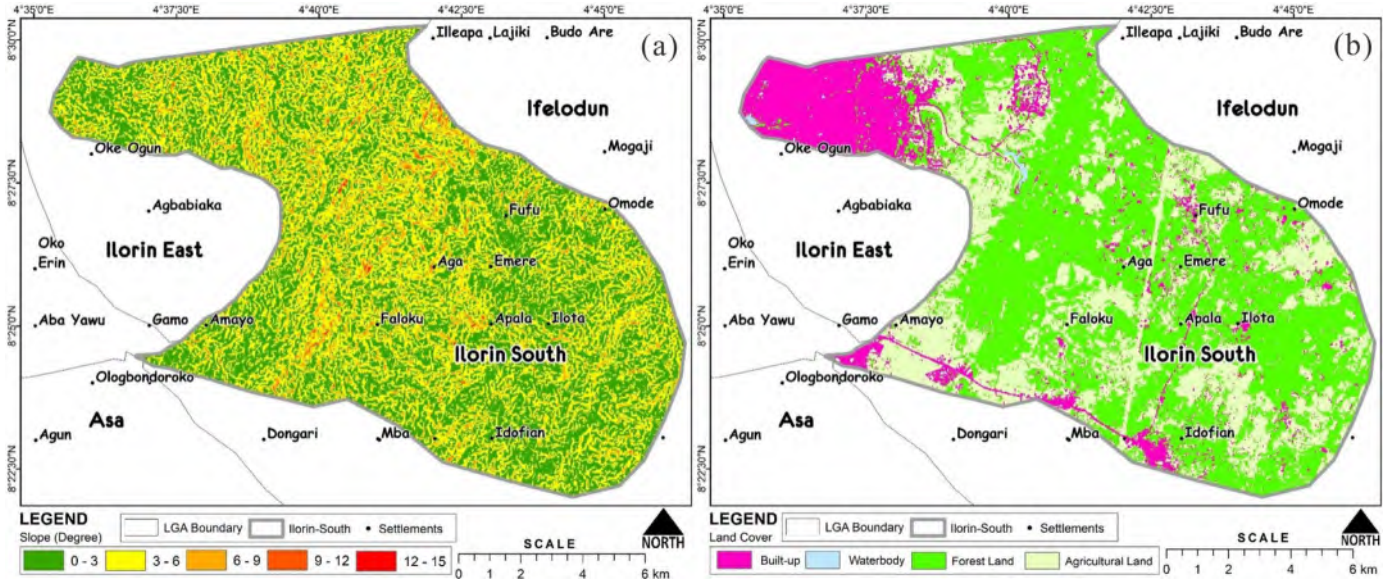

Fig. 4. (a) Slope map in the study area with the resulting raster values classified into five categories: 0-3°; 3-6°; 6-9°; 9-12°; 12-15° with the greater part of the study area having low slope, and (b) land use/land cover map of the study area prepared using remote sensing data of Landsat 8. After classification using supervised classification tool four classes corresponding to the built-up, waterbody, forest land, and agricultural land were found.

saline water in the case of hyporheic zones (surface-groundwater interface) or points from where planned or unplanned release of anthropogenic contaminants can seep into groundwater reservoirs. Topographic data could be in the form of elevation and slope (from DEM), relief (contour lines on maps), drainage patterns (rivers, streams) and geographical positions. A gentle slope reduces the speed of surface runoff which in turn increases the rate of infiltration in the ground while a steep slope reduces the rate of water infiltration into the ground (Silwal and Pathak, 2018). This means that slope is among the factors that influence the infiltration of water into the ground. The rate of infiltration of surface water is inversely related to the slope (Prasad et al., 2008). The slope map shows that the slope varies between 0 and 15° and the whole of Ilorin South is dominated by a very gentle slope (<5°). This confirms the suitability of this layer for groundwater recharge provided all other contributory layers to groundwater recharge (lineaments, soil, drainage and rainfall) are also favourable.

4.1.4. Land use/land cover (LULC)

The land use/land cover map of the study area grouped into four classes (i.e., water body, built-up area/settlement, agricultural land and forest land) is shown in Fig. 4b. LULC gives urban impressions and is an indicator of anthropogenic influences and their possible impacts on the hydrogeology of any zone (Jesiya and Gopinath, 2019). The map shows that the area is dominated by forest land covering roughly 60% of the area. This is followed by the other classes. In WRA, LULC data serves a dual purpose; it is a socio-economic dataset that enriches us with the understanding of the water needs, and at the same time it can serve as topographic data giving us ideas of agricultural zones, forests, cities, industrial zones etc. As a result, soil formation and groundwater infiltration procedures are subject to the type of LULC as it also affects the water distributions for different uses. Land cover can give an idea of the total component of rainfall that would be infiltrated, the capability of the land for surface runoff and erosion, and the degree of potential evapotranspiration of the land investigated. There is a higher infiltration rate in the areas covered by agricultural land and forest land. The water body is considered a source of groundwater recharge (Agarwal and Garg, 2016). According to Jimoh (2011), grasslands are the most potent for checking the incidence of erosion in Ilorin due to the ability of the grasses to break the impact of rainfall at ground level thereby rendering the power of rainfall almost insignificant (the intensity and duration of rainfall events in Ilorin is not high due to the semi-arid climate). Ilorin South is still largely a natural environment except for the university landmass which is a built-up area. There are grasses and shrubs to curtail the effect of erosion and runoff. Table 6 shows the LULC accuracy assessment matrix (ground truth versus predicted). The overall accuracy of the classification is 72.22%.

4.1.5. Rainfall

Rainfall is a hydro-meteorological variable and its essence is to define the characteristics of the available resources. Some of the climatic factors are precipitation, temperature, humidity, solar radiation and wind speed. While precipitation gives an idea of the rechargeability of groundwater zones, the other four factors enable the estimation of evaporation. In locating groundwater recharge zones of an area, precipitation (especially rainfall) and drainage distribution network contribute significantly. Rainfall determines the amount of water that would be available for infiltration into the groundwater system (Agarwal and Garg, 2016). A run of Pearson's correlation analysis shows that the PERSIANN and NiMet datasets are positively correlated ($r = 0.67$). This confirms that both datasets exhibit similar trends in rainfall patterns and gives credence to the adoption of PERSIANN as the primary rainfall dataset for the study. The resulting rainfall distribution map produced from the interpolation of all rainfall data of different locations is shown in Fig. 5a. The mean annual rainfall is grouped into four classes ranging from 2010-2170 mm. It is observed that the south-eastern part receives the highest amount of rainfall, while the north-western part recorded the least rainfall. Generally, the contribution of rainfall to groundwater availability in the zone is insignificant as the region is known for its aridity (Ashaolu and Iroye, 2018). Thus, from the rainfall distribution map, the UNILORIN active area (NNW) is characterised by semi-arid rainfall with a mean annual rainfall of 2010-2170 mm. This implies that the contribution of rainfall to groundwater availability in the zone is insignificant because the region is semi-arid and characterized by rainwater deficit. According to Ashaolu and Iroye (2018), the parts of Ilorin closer to the western littoral hydrological zone of south-

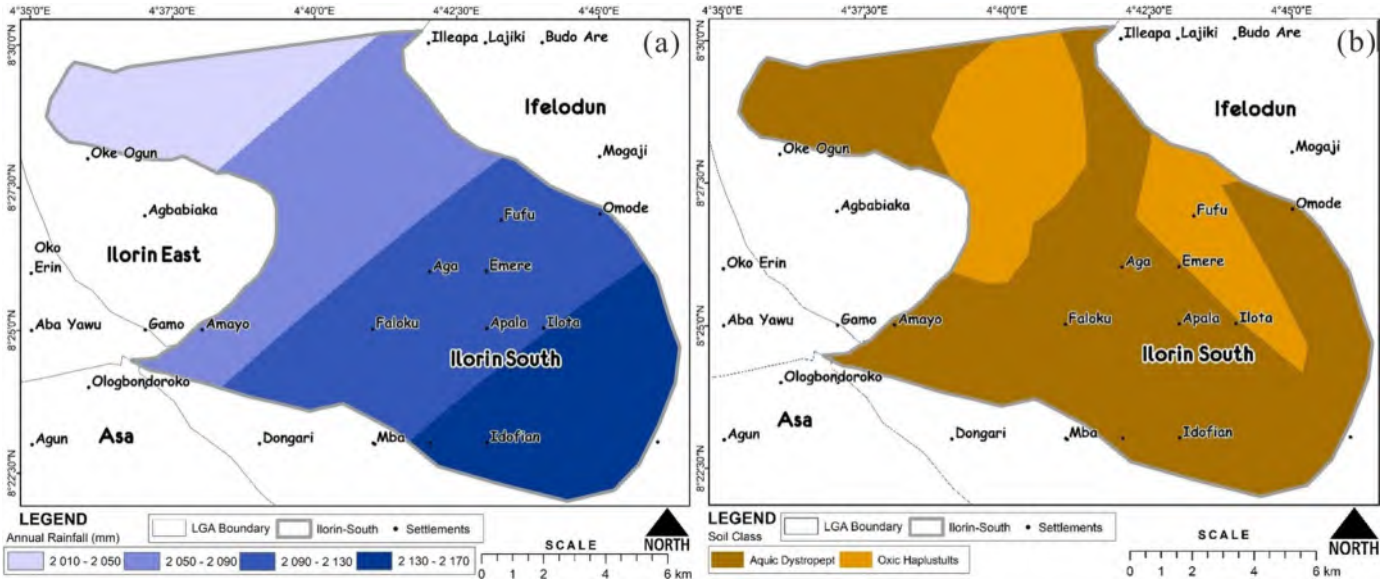

Fig. 5. (a) Rainfall map estimated the amount of precipitation into the ground. Four main rainfall classes are recorded over the study area. The first rainfall class covered the western and received the lowest amount of rainfall and the southern part received the highest amount (b) soil type map of the study area reveals two main soil categories: aquic dystropept (clayey) and oxic haplustults (laterites). The aquic dystropepts are soils with aquic (water) conditions and will hold water only during the wet seasons due to the low base saturation. The Oxic haplustults are red-to-yellow soils of clay accumulation vulnerable to evaporation.

western Nigeria have a moderate aridity index and are referred to as dry sub-humid, but from Ilorin Central to the northern border of Ilorin is semi-arid and as a result, water shortages are experienced annually.

4.1.6. Soil

Soils refer to unconsolidated minerals or organic matter on the surface which can either be liquid or gas (wet or dry soils) and are not beyond 200 cm from the surface (WMO, 2012). The classification by the Food and Agriculture Organization (FAO), and United Nations Educational Scientific and Cultural Organization (UNESCO) differentiates 28 major soil groups and a total of 153 soil units (ISRIC, 1994; WMO, 2012). Another commonly adopted soil classification is the United States Department of Agriculture (USDA) classification which to a large extent is a derivation of the FAO-UNESCO classification. As shown in Fig. 5b, the study site is covered principally by two forms of alternating soils which according to the USDA soils taxonomy are “aquic dystropept (clayey)” and “oxic haplustults (laterites)” (Nwachokor and Uzu, 2008). According to a combination of assimilated knowledge of FAO-UNESCO and USDA taxonomy, aquic dystropepts are soils with aquic (water) conditions, moderately developed soils with limited pedogenetic age because of rejuvenation of soil materials and they usually have low base saturation. Oxic haplustults are red-to-yellow soils of clay accumulation with minimum and simple horizon development, strongly leached, low cation exchange capability, low base saturation, and underlain by acid parent rocks (ISRIC, 1994). Although these soils differ in their physical characteristics and permeabilities, they are both not favourable to groundwater infiltration and percolation. Thus, around the UNILORIN flanks, the aquic parts will hold water only during the wet seasons due to the low base saturation, and the oxics are vulnerable to evaporation. Both soil types are not adding significant recharge to the aquifers in the zone.

4.1.7. Drainage

Drainage maps are used to characterize the water flow direction and accumulation in catchments. The drainage density map is shown in Fig. 6a. It reveals that Ilorin South is dominated by low drainage density and thus, surface runoff is minimal. Consequently, there is a high potential for water (precipitation or irrigation) retention which will aid groundwater recharge.

4.2. Analysis of groundwater potential zones

Fig. 6b shows the Groundwater Potential Zones (GWPZ) map of Ilorin South LGA. The groundwater potentiality is zoned into three classes of low, moderate and high potential. The zonation map shows that the area is dominated by the moderate potential class covering an area of 100.46 km^2 which constitutes 60.6% of the study area. The high potential class covers an area of 9.73 km^2 which is about 5.9% of the study area. Also, the low potential class occupies an area of about 55.48 km^2 or 33.5%.

4.3. Interpretation of derivatives

The results of the processed aeromagnetic data of Ilorin South are presented as derivatives maps in Figs. 7-9. These include the residual magnetic intensity (RMI) map, reduced to equator (RTE) map, first and second vertical derivative maps (FVD and SVD), and analytic signal (AS) map. These maps were used to process the magnetic data and provide information on the structural settings (i.e., edge location and boundaries) and tectonic trends of an area (Srivastava and Agarwal, 2010; Skiba et al., 2016; Balogun, 2019). Structural information that could be obtained through the application of edge detection techniques to the aeromagnetic data are lithological contacts, faults and dykes (or pre-tertiary intrusives). These structures guide the evaluation of geologic hazards, act as traps for hydrocarbons, and are controls for the movement/accumulation of groundwater especially in the basement terrain (Ejepu et al., 2017; Ishola et al., 2020). The deeper magnetic sources characterised by low magnetic amplitudes are probably of Precambrian basement rocks while shallow magnetic sources associated with high magnetic amplitudes depict basic intrusives and/or magnetised bodies within the sedimentary cover and shallow subsurface (Ozebo et al., 2017; Ibraheem et al., 2019).

The first and second vertical derivatives (FVD and SVD) show litho-contrasts, while the AS map shows more sundry magnetic

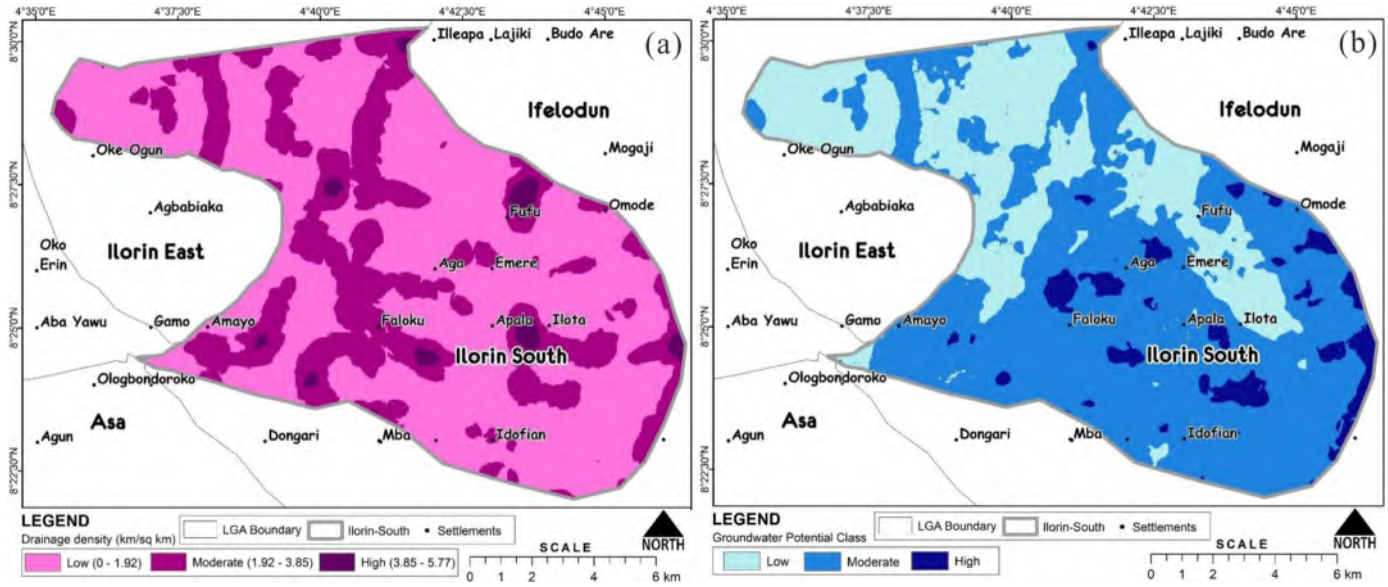

Fig. 6. (a) Drainage density map shows how lithology with major and minor fractures controlling the groundwater systems. The drainage density map is grouped into three classes. They are low (0-1.92), medium (1.92-3.85) and high (3.85-5.77). (b) Groundwater potential zones (GWPZ) map of Ilorin South LGA. The map is classified into three classes: high (5.9%), moderate (60.6%), low (33.5%).

bodies (intrusions/basement uplift; Ozebo et al., 2017). According to Skiba et al. (2016) and Ibraheem et al. (2019), strongly magnetic rocks generally include basalts and gabbro, while rocks like granite, granodiorites and rhyolites have only moderately high magnetic susceptibilities. The known common causes of magnetic anomalies are the intrusion of mafic and ultramafic dykes, sills, lava flows and magnetic ore bodies. Based on magnetic signatures, the aeromagnetic data reveals that the study area is underlain with volcanics of porphyritic texture and seriated fabric (details in Skiba et al., 2016; Ibraheem et al., 2019). The main magnetic anomalies are located within the NW zone while the other anomalies are seen towards the SE trend.

From the residual magnetic intensity map (Fig. 7a), hard rocks (Mafic igneous/volcanics) with magnetic amplitudes that span from 78.4 to 109.9 nT and Felsic igneous/volcaniclastics with amplitude values of 21.8 to 71.0 nT which are interwoven with sediments having amplitudes between -89.2 to 12.1 nT are delineated. The regions with negative anomalies (variants of blue colours) are sediments, troughs or places where faults have dropped down the basement or other structures. Alternating positive anomalies are largely created by irregularities in the buried basement rocks beneath sedimentary covers. The upper region of the study area that trends NE-SW consists of igneous rocks, although shallow ($\leq$75.1 nT on RTE and $\leq$78.4 nT on RMI), is uniformly extensive and shows no sign of lithologic contrasts or discontinuity (possible structures) except for the edges around Ile-Apa that show visible structures and sedimentary basement.

The RTE map of the gridded TMI is shown in Fig. 7b. The map reveals the general delineated structural trends in the studied area that are observed mainly in the north-western part with high magnetic amplitudes relative to the southern part. The differentiated magnetic lithological contact follows from lineation in magnetic sources which could be linked with intrusive features or surfaces of fractures in the basement topography important for groundwater assessment.

The first vertical derivative map is shown in Fig. 8a and second vertical derivative map in Fig. 8b reveal dominant magnetic anomalies in the region and they trend NE-SW and approximately N-S. These linear features which are seen in both derivative maps are associated with faults /fractures occurrence in the region. The AS map which gives the total gradient in depth dimension is shown in Fig. 9. A large part of the sheet is underlain with volcanics of porphyritic texture and seriated fabric (Ejepu et al., 2015; Skiba et al., 2016; Ibraheem et al., 2019). The depth to the magnetic basement ranges from 244 to 1703 m for shallow and deep magnetic sources respectively. The abrupt change in depth suggests that the magnetic basement in the easternmost region has been downthrown relative to the westernmost region. This deduction agrees with previous geological studies within the studied area revealing that the area is underlain with granite suite (foliated granodiorite, foliated micro granites and older granites), gneiss complex (augen gneiss, banded gneiss and granite gneiss), and pegmatite and quartz veins (Olasehinde and Raji, 2007; Raji and Bale, 2008) all of which have low to moderately high magnetic susceptibilities and are always difficult to fracture especially the granitic masses. The aeromagnetic data processed by the application of filter algorithms has shown the position, boundaries, and extent of the magnetic structures that might control the groundwater flow in the area.

The lineaments delineated from the magnetic survey validate the remotely sensed lineaments pointing to the fact that most parts of the areas of interest have moderate groundwater potential clusters (light blue areas) with pockets of low potential areas (sky blue spots) distributed around the area. Only a small area has high groundwater potential (deep blue) within the studied regions.

4.4. Validation and discussion

Denser lineament zones indicate that the intensity of the rock fracturing system required for the development of fissures and channels for the movement of groundwater (Mogaji et al., 2011). From the lineaments map shown in Fig. 3b and Fig. 10, it can be observed that the north-western part that coincides with most of the area of interest consists of low surficial lineaments. It is potentially a weak zone and subsurface fractures that could serve as passage or conduits for groundwater might not be present. However, the central and south-eastern parts of the study area (i.e., Aga, Emere, Faloku, Fufu, Ga Gata, Idofian, Ilota, and the borders of Ilorin South with Amoyo and Ifelodun) have moderate to high lineament density. As a result, they are potentially high zones for

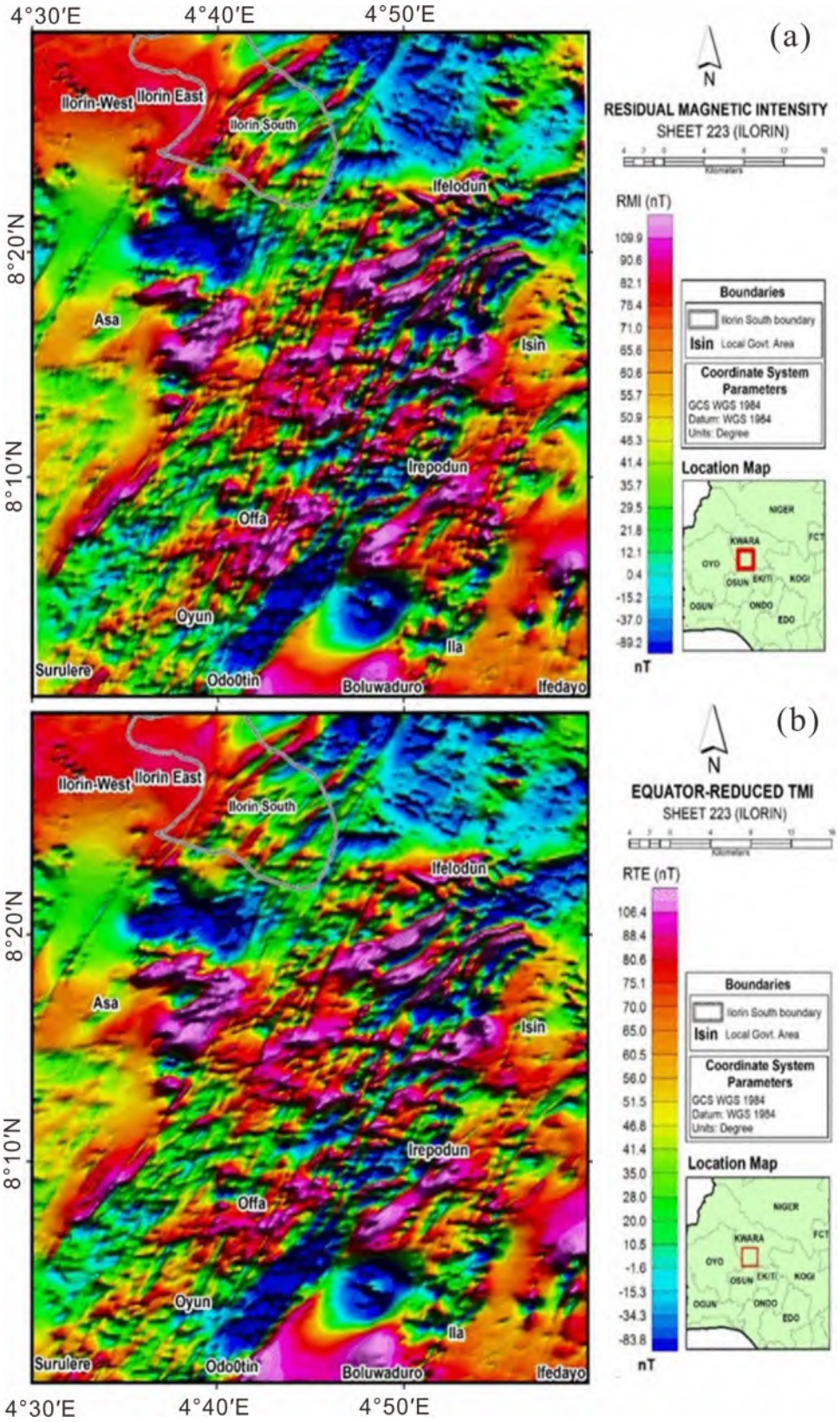

Fig. 7. (a) Residual magnetic intensity map of the TMI with three regions clearly obvious. The high amplitude anomalies (reddish purple), moderate amplitude anomalies (greenish yellow), and low amplitude anomalies (blue) and (b) reduced to equator map of the gridded TMI shows the location of the observed magnetic anomalies directly over the magnetic source bodies that caused the anomaly. The RTE map shows both low magnetic frequency representing low magnetic signature (blue) and high magnetic frequency suggesting points of high magnetic signatures (purple) in the area.

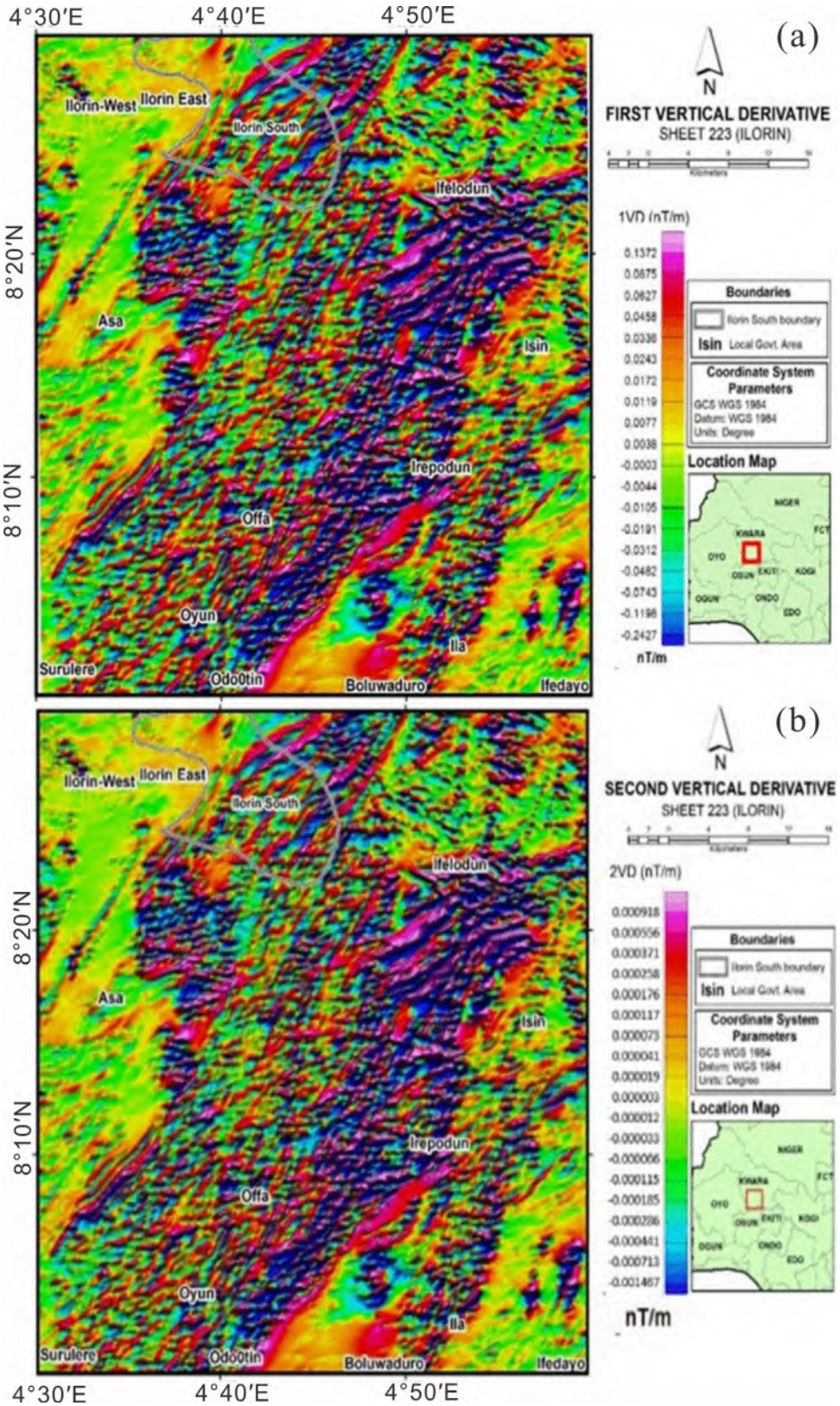

Fig. 8. (a) First vertical derivative map shows the basement structural features with subtle lineaments. They are gradient zones, alignment of different local anomalies with different discontinuities on the anomaly pattern and (b) second vertical derivative map further enhanced the magnetic anomalies boundaries with dominant magnetic anomalies in the region trending NE-SW and approximately N-S. The linear features which are linked to the fractures in the study area.

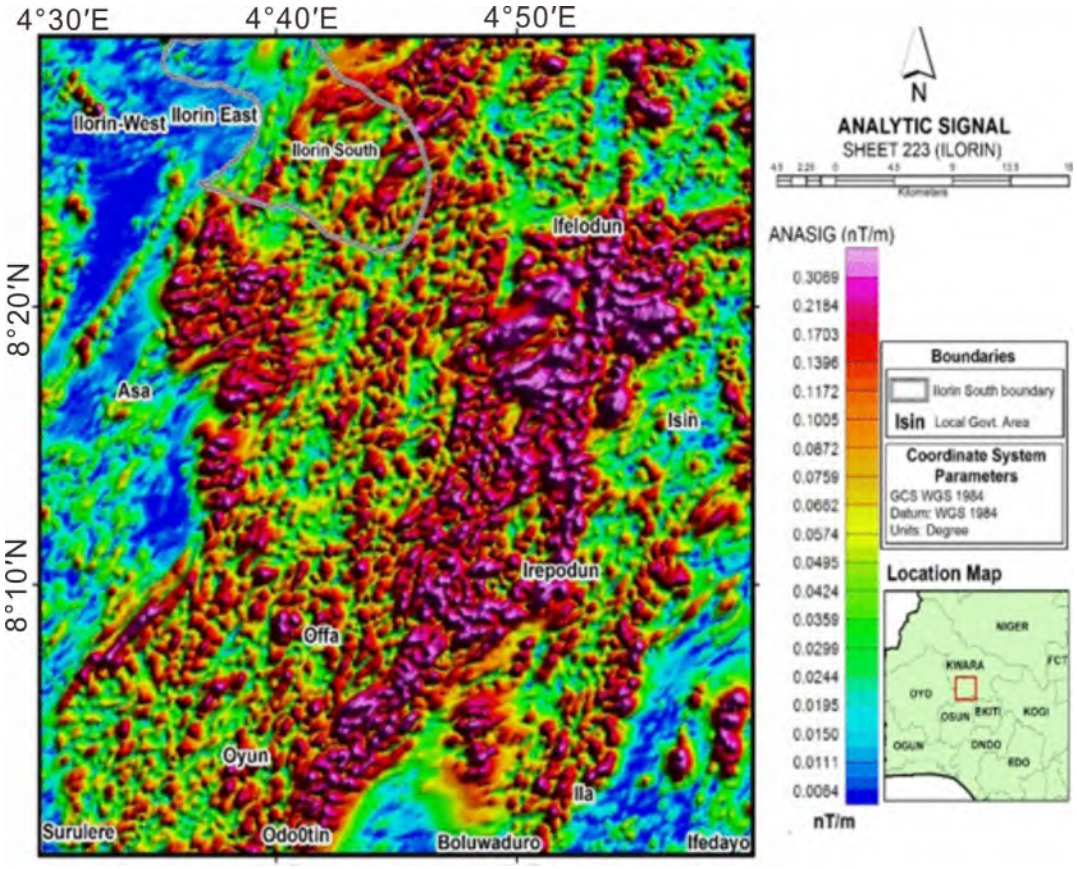

Fig. 9. Analytic signal map reveals N-S structures and confirmed the existence of lineaments or rock boundaries in the study area. The near surface anomalies with magnitude between 0.0054-0.0495 nT/m (blue).

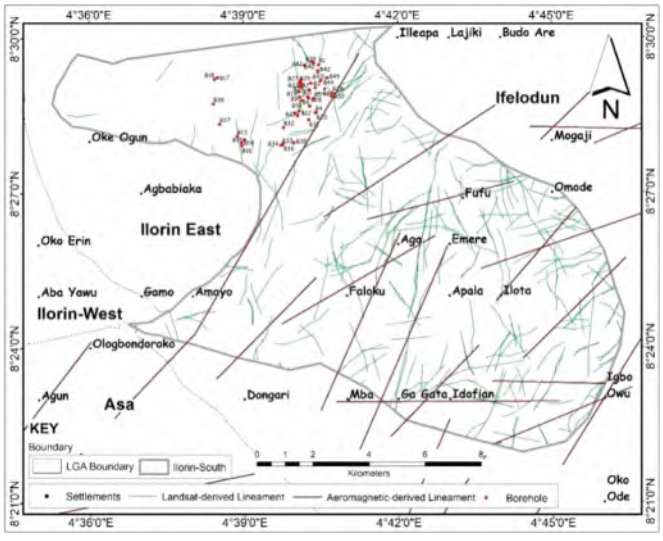

Fig. 10. Superposition of Landsat-derived lineaments and magneto-lineaments. Cross-cutting or intersecting lineaments with orientations in different directions are clearly obvious. The low lineament densities are dominant in the studied area.

groundwater yield and extraction (Ejepu et al., 2015, 2017). The result of overlaying the Landsat-derived lineaments and magnetic lineaments is shown in Fig. 10. It clearly shows some cross-cutting or intersecting lineaments with orientations in different directions. Generally, low lineament densities are dominant in the studied area with chances of low groundwater accumulation arising from low porosity and permeability.

In comparison with the remote sensing data, the aeromagnetic data have a higher depth of investigation (Reeves, 1989) and precision due to differences in altitudes. More so, the magnetic lineaments reveal potential faults, deep fractures and intrusive bodies which are structural features for groundwater repositories mapping in the basement regions. This explains the presence of more image lineaments in Fig. 10 (since not all image lineaments are magnetic) than magneto-lineaments (Ranganai and Ebinger, 2008; Muthamilsevan et al., 2017). The remote sensing data reveals surface or image lineaments that are surficial reaching a depth of about 1-10 m (WMO, 2012) that could suggest recharge zones for groundwater (Ejepu et al., 2017). This corroborates why aeromagnetic surveys are increasingly being used for regional and subregional spatial confirmation and ground validation (ground truth) of remote sensing data (Grauch and Bankey, 2003; Adiat et al., 2013; Muthamsilselvan et al., 2017). Even though aeromagnetic data has limitations in detecting the presence of water, contrasts in magnetic properties of some peculiar rock types can be sensed to deduce many subsurface geologies that control the presence, quality and flow of groundwater (Grauch and Bankey, 2003). Geological features such as faults are identified on a magnetic map where magnetic contrast and abrupt changes in magnetisation within rock units are visible. This is due to the structural juxtaposition of litho-units produced by the primary difference in magnetisation or due to the secondary destruction or growth of magnetic materials (Grauch and Bankey, 2003; Ranganai and Ebinger, 2008). Thus, the integration of remotely sensed data and geophysical data (e.g., aeromagnetic) gives a synoptic view of the study area, far beyond the capability of depth probing methods such as electrical imaging. This is important in the assessment phase where the focus is the regional understanding of geologies and geomor-

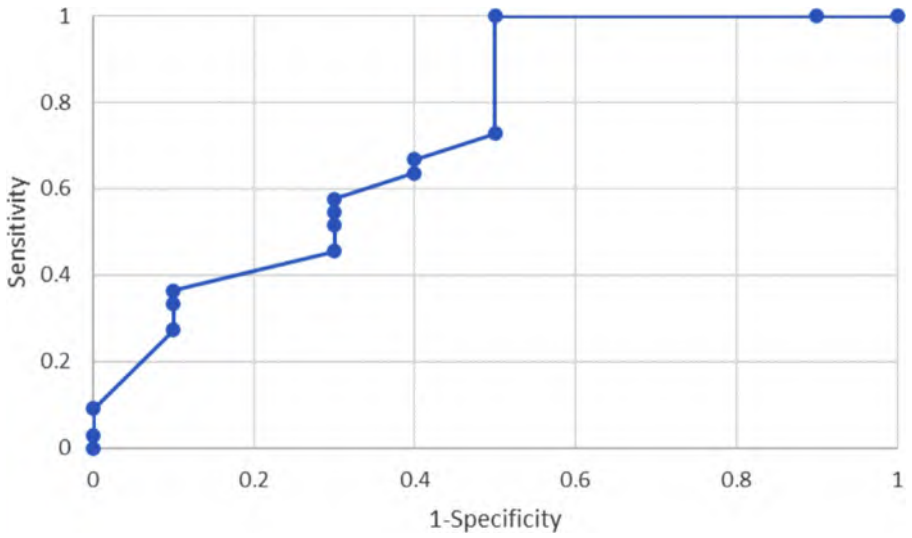

Fig. 11. ROC curve for groundwater potential index predictive map shows the relationship between the sensitivity and specificity of the groundwater potential model indicating satisfactorily good accuracy in the spatial prediction of the groundwater potentiality.

Table 5
Normalized weights of the final selected thematic layers and sub-classes.

Thematic layer	Normalized priority weight	Class	Assigned weight	Normalized weight	Area (km^2)
Drainage density (km/km^2)	0.2429	Low	1	0.1667	110.99
		Moderate	2	0.3333	51.28
		High	3	0.5000	3.38
Lineament density (km/km^2)	0.1964	Low	1	0.1667	106.88
		Moderate	2	0.3333	49.93
		High	3	0.5000	8.83
Land cover	0.1689	Waterbody	4	0.4000	0.32
		Agricultural land	3	0.3333	54.97
		Forest land	2	0.2000	86.83
		Built-up area	1	0.1000	23.53
Soil class	0.1413	Aquic Dystropept	2	0.6667	121.88
		Oxic Haplustults	1	0.3333	43.78
Annual rainfall (mm)	0.1071	2010-2050	1	0.1000	24.92
		2050-2090	2	0.2000	46.27
		2090-2130	3	0.3333	57.48
		2130-2170	4	0.4000	36.97
Slope (°)	0.0891	0-3	5	0.3333	73.36
		3-6	4	0.2667	71.28
		6-9	3	0.2000	11.71
		9-12	2	0.1300	0.85
		12-15	1	0.0700	0.04
Geomorphology	0.0541	Plain	3	0.5000	11.45
		Lowland	2	0.3333	128.04
		Upland	1	0.1667	26.17

phologies for easy, quick, and cheap decision-making, especially in Precambrian basement rocks. For validating the remotely sensed data, the lineaments intersection has been highlighted to be a pointer to groundwater exploration (Epuh et al., 2020). In such zones, both porosity and permeability will be very high which can act as hard rock aquifer parameters/characteristics for groundwater (Muthamsilselvan et al., 2017).

Table 7 shows the borehole status and corresponding GWPI used in the validation with ROC curves. Also, a summary of the computed ROC statistics is presented in Table 8 while Fig. 11 displays the ROC curve. The AUC value for this study is estimated to be 0.73. This implies a predictive (satisfactory) accuracy of 73% for the developed groundwater potential zone map. Thus, the GWPZ map resulting from this study could provide relevant information to stakeholders in the groundwater resources management of the study area.

5. Conclusion

In this study, a GWPZ map was developed for Ilorin South LGA with emphasis on UNILORIN, north-central, Nigeria using the integration of remote sensing, geospatial and aeromagnetic datasets to understand the groundwater conditions in the studied area. Seven thematic layers which served as groundwater controlling factors were identified, overlaid, and analysed. The north-western part of the study area consists of low surficial lineaments, and conduits for groundwater might not be present in that zone. However, the central and south-eastern parts of the study area have moderate to high lineament density, and are potentially high in groundwater potential. The study area was classified into three zones of low, moderate, and high potential. The high zone indicated the most suitable region for groundwater prospect while the low zone also depicted the least favourable area. The correlation of the GWPZ

Table 6
Land cover accuracy assessment matrix: ground truth vs. predicted.

Land cover class		Ground truth image				
		Built-up area	Water body	Forest land	Agricultural land	Total
Predicted	Built-up area	5	0	1	1	7
	Water body	0	4	0	0	4
	Forest land	0	0	12	12	24
	Agricultural land	0	0	1	18	19
	Total	5	4	14	31	54

Table 7
Borehole status, coordinates, GWPI and GWPZ.

Borehole ID	Status	Lat (°N)	Long (°E)	GWPI	GWPZ
1	Functional	8°29′28"	4°40′27"	0.214767	Low
2	Dysfunctional	8°29′03"	4°29′41"	0.228118	Low
3	Dysfunctional	8°29′02"	4°40′23"	0.226920	Low
4	Functional	8°28′33"	4°40′23"	0.232005	Low
5	Functional	8°28′49"	4°40′22"	0.217103	Low
6	Functional	8°28′40"	4°40′17"	0.222230	Low
7	Functional	8°29′03"	4°40′05"	0.213933	Low
8	Dysfunctional	8°29′06"	4°40′07"	0.213780	Low
9	Functional	8°28′51"	4°40′05"	0.223185	Low
10	Functional	8°28′46"	4°40′07"	0.243051	Low
11	Dysfunctional	8°28′51"	4°40′14"	0.218909	Low
12	Functional	8°28′35"	4°40′04"	0.235679	Low
13	Dysfunctional	8°28′05"	4°38′52"	0.215741	Low
14	Dysfunctional	8°27′58"	4°38′57"	0.225091	Low
15	Functional	8°28′01"	4°39′01"	0.222859	Low
16	Dysfunctional	8°27′01"	4°38′01"	0.226820	Low
17	Functional	8°29′14"	4°38′29"	0.262727	Low
18	Functional	8°29′12"	4°38′26"	0.261089	Low
19	Dysfunctional	8°28′57"	4°40′04"	0.217627	Low
20	Functional	8°28′33"	4°40′24"	0.230173	Low
21	Functional	8°28′29"	4°40′03"	0.237697	Low
22	Functional	8°28′32"	4°40′00"	0.243500	Low
23	Functional	8°29′05"	4°40′07"	0.214680	Low
24	Functional	8°29′06"	4°40′07"	0.213874	Low
25	Functional	8°29′08"	4°40′05"	0.214302	Low
26	Functional	8°29′09"	4°40′06"	0.216726	Low
27	Functional	8°29′11"	4°40′06"	0.215415	Low
28	Functional	8°28′50"	4°40′16"	0.217188	Low
29	Unconfirmed	8°28′55"	4°40′43"	0.267987	Low
30	Unconfirmed	8°28′52"	4°40′42"	0.276051	Moderate
31	Unconfirmed	8°28′24"	4°40′16"	0.228046	Low
32	Functional	8°28′16"	4°39′46"	0.247296	Low
33	Functional	8°27′55"	4°39′44"	0.240535	Low
34	Functional	8°27′55"	4°39′43"	0.238319	Low
35	Unconfirmed	8°27′05"	4°39′58"	0.286843	Moderate
36	Functional	8°27′57"	4°39′46"	0.242117	Low
37	Functional	8°28′19"	4°38′31"	0.257201	Low
38	Functional	8°28′43"	4°38′24"	0.267354	Low
39	Functional	8°29′30"	4°40′21"	0.212858	Low
40	Functional	8°29′32"	4°40′20"	0.206257	Low
41	Functional	8°29′28"	4°40′11"	0.239098	Low
42	Functional	8°29′21"	4°40′26"	0.218971	Low
43	Functional	8°29′20"	4°40′27"	0.212962	Low
44	Functional	8°29′10"	4°40′30"	0.217870	Low
45	Functional	8°29′13"	4°40′37"	0.218354	Low
46	Functional	8°29′07"	4°40′18"	0.219724	Low
47	Functional	8°28′59"	4°40′16"	0.220665	Low

map with the aeromagnetic maps gives satisfactory results. It follows that Ilorin South LGA has a moderate-to-high groundwater potential while the area coinciding with the UNILORIN landmass has low-to-moderate groundwater potential. Thus explains the scarcity in water supply being experienced in UNIILORIN.

In comparison with the remote sensing data, the aeromagnetic data have a higher depth of investigation. The remote sensing data reveals surface or image lineaments that are surficial and that could suggest recharge zones for groundwater. This corroborates why aeromagnetic was used in this study for spatial confirmation and ground validation (ground truth). Summarily, the integration of remotely sensed data and aeromagnetic data provided a synoptic view of the study area. This is important in the assessment phase where the focus is the regional understanding of geologies and geomorphologies for easy, quick, and cheap decision-making, especially in Precambrian basement rocks.

Many countries cannot depend solely on groundwater to meet the increasing demands of their people for domestic and other uses. The need to harness a combination of boreholes, municipal water, and dams for optimal supply becomes necessary. GWPZ maps are useful guide for decision-making with regard to sustainable groundwater development and management (Table 5).

Table 8
A summary of ROC statistics - Area Under the Curve (AUC).

Area	Std. Error	Asymptotic Sig.	Asymptotic 95% Confidence Interval	
			Lower Bound	Upper Bound
0.730	0.101	0.029	0.532	0.929

Declaration of Competing Interest

The authors declare no conflict of interest.

Acknowledgements

The authors acknowledge the support of Mr. Tomiwa Akanbi (Nigerian Geological Survey Agency, Abuja), Mr. Yussuf Hammed (Physics Department, Kinsey College of Education, Ilorin), Surveyor Ipadeola (Surveying and Geoinformatics Department, UNILORIN) and Professor C.O. Akoshile (Physics Department, UNILORIN and former director of UNILORIN Renewable Energy Centre – UREC). Also, appreciation goes to Professor P.C. Nwilo, Department of Surveying & Geoinformatics, University of Lagos (UNILAG) for giving the researchers free access to the facilities in the Remote Sensing and Photogrammetry Laboratory of the Department. We sincerely appreciate Mr. Samuel Akinnusi of UNILAG's Surveying and Geoinformatics Department for his help and support in the Remote Sensing/Photogrammetry lab. Ultimately, we say a big thanks to the Director of the University of Ilorin Works Department for giving detailed information on some of the school infrastructure, especially in connection to water resources. We are grateful to the anonymous reviewers for their insightful comments which immensely improved this manuscript.

References

Abu El-Ata, A.S., El-Khafeef, A.A., Ghoneimi, A.E., Abd Alnabi, S.H., Al-Badani, M.A., 2013. Applications of aeromagnetic data to detect the basement tectonics of Eastern Yemen region. Egypt. J. Pet. 22, 277–292.

Adelana, S.M., 1988. Seismic refraction survey of UNILORIN main campus, unpublished M.Sc. Thesis. University of Ilorin, Kwara State, Nigeria.

Adiat, K.A.N., Nawawi, M.N.M., Abdullah, K., 2012. Assessing the accuracy of GIS-based elementary multi-criteria decision analysis as a spatial prediction tool – A case of predicting potential zone of sustainable groundwater resources. J. Hydrol 440-441, 75–89.

Adiat, K.A.N., Nawawi, M.N.M., Abdullah, K., 2013. Application of multicriteria decision analysis to geoelectric geologic parameters or spatial prediction of groundwater resources potential aquifer evaluation. Pure. Appl. Geophys. 170, 453–471.

Agarwal, R., Garg, P.K., 2016. Remote Sensing and GIS-based groundwater potential recharge zones mapping using multi-criteria decision-making technique. Water Resour Manage 30, 243–260.

Ahmad, A., Quegan, S., 2012. Analysis of maximum likelihood classification on multispectral data. Appl. Math. Sci. 6 (129), 6425–6436.

Ahner, B., 2013. Assessing groundwater stress: An approach of measuring groundwater stress based on sub-national statistical data; IGRAC, Westvest 7, The Netherls.

Ajibade, A.C., Woakes, M., Rahaman, M.A., 1987. Proterozoic crustal development in the Pan-African regime of Nigeria. Proterozoic Lithospheric Evolution Dynamics 77, 259–271.

Akinlalu, A.A., Adegbuyiro, A., Adiat, K.A.N., Akeredolu, B.E., Lateef, W.Y., 2017. Application of multi-criteria decision analysis in prediction of groundwater resources potential: A case of Oke-Ana, Ilesa, South-Western Nigeria. NRIAG J. Astron. Geophys. 6, 184–200.

Alademomi, A.S., Okolie, C.J., Daramola, O.E., Agboola, R.O., Salami, T.J., 2020. Assessing the relationship of LST, NDVI and EVI with L Cover changes in the Lagos Lagoon environment. Quaestiones Geographicae 39 (3), 87–109 Bogucki Wydawnictwo Naukowe, Poznań.

Amadi, A.N., Olasehinde, P.I., 2010. Application of remote sensing techniques in hydrogeological mapping of parts of Bosso Area, Minna, North-Central Nigeria. Int. J. Phys. Sci. 5 (9), 1465–1474.

Anderson, J.R., Hardy, E.E., Roach, J.T., Witmer, R.E., 1976. A land use and land cover classification system for use with remote sensor data. Geological Survey Professional Paper 964. https://pubs.usgs.gov/pp/0964/report.

Anifowose, A.Y.B., Aladejana, O.O., 2015. A preliminary assessment for groundwater in a part of North-Central Nigeria using Lsat ETM. Glob. J. Geol. Sci. 14, 1–12 ISSN: 1596-6798.

Anuforom, C.A., 2013. Induction lecture of Nigeria academy of science. Nigeria Meteorological Agency (NiMet), Oshodi, Lagos-Nigeria.

Arisona, A., Ishola, K.S., Nawawi, M.N.M., 2020. Subsurface void mapping using geophysical and geotechnical techniques with uncertainties estimation: case study of Kinta Valley, Perak, Malaysia. SN Appl. Sci. 2, 1171.

Ashaolu, E.D., Iroye, K.A., 2018. Rainfall and potential evapotranspiration patterns, their effects on climate water balance in the western littoral hydrological zone of Nigeria. Ruhuna J. Sci 9 (2), 92–116.

Balogun, O.B., 2019. Tectonic and structural analysis of the Migmatite-Gneiss-Quartzite complex of Ilorin area from aeromagnetic data. NRIAG J. Astron. Geophys. 8 (1), 22–33.

Black, R.R., Caby, R., Moussine-Pouchkine, A., Bayer, R., Bertr, J.M., Boullier, A.M., Fabre, J., Lesquer, A., 1979. Evidence for late Precambrian plate tectonics in West Africa. Nature 278, 223–227.

Brunelli, M., 2015. Introduction to the Analytic Hierarchy Process, 83. Springer Briefs in Operations Research.

Caby, R., 1989. Precambrian terrains of Benin, Nigeria and Northeast Brazil: the late Proterozoic South Atlantic fit. Geol. Soc. Am. Special Paper 230, 145–158.

Carter, J.V., Pan, J., Rai, S.N., Galiuk, S., 2016. ROC-ing along: Evaluation and interpretation of receiver operating characteristic curves. Surgery 159 (6), 1638–1645.

Centre for Hydrometeorology and Remote Sensing (CHRS), 2019. Data portal for PERSIANN (precipitation estimation from remotely sensed information using artificial neural network) global satellite precipitation events.

Coscia, I., Linde, N., Greenhalgh, S., Vogt, T., Green, A., 2012. Estimating travel times of groundwater flow patterns using 3D time-lapse crosshole ERT imaging of electrical resistivity fluctuations induced by infiltrating river water. Geophysics 77 (4), E239–E250.

Dada, S.S., 2008. Proterozoic evolution of the Nigeria – Boborema province. Geol. Soc. Spec. Publ. 294, 121–136.

Ejepu, S.J, Olasehinde, P.I., Omar, D.M., Abdullahi, D.S., Adebowale, T.A., Ochimana, A., 2015. Integration of geology, remote sensing and GIS in assessing groundwater potential of Paiko sheet 185 North-central Nigeria. J. Inf. Educ. Sci. Tech. (JIEST). 2 (1), 145–155.

Ejepu, J.S., Olasehinde, P.I., Okhimamhe, A.A., Okunlola, I., 2017. Investigation of hydrogeological structures of Paiko region, North-central Nigeria using integrated geophysical and remote sensing techniques. Geosciences 7, 122.

Elbeih, F.S., 2015. An overview of integrated remote sensing and GIS for groundwater mapping in Egypt. Ain Shams Eng. J. 6, 1–15.

El-Sawy, E.K., Ibrahim, A.M., El-Bastawesy, M.A., El-Saud, W.A., 2016. Automated, manual lineaments extraction geospatial analysis for Cairo-Suez district (Northeastern Cairo-Egypt), using remote sensing and GIS. Int. J. Innov. Sci. Eng. Technol. 3 (5), 491–500.

Epuh, E.E., Okolie, C.J., Daramola, O.E., Ogunlade, F.S., Oyatayo, F.J., Akinnusi, S.A., Emmanuel, E.I., 2020. An integrated lineament extraction from satellite imagery and gravity anomaly maps for groundwater exploration in the Gongola basin. Remote Sens.Appl.: Soc.Environ 20, 100346. doi:10.1016/j.rsase.2020.100346, 12.

Fashae, O.A., Tijani, M.N., Talabi, A.O., Adedeji, O.I., 2013. Delineation of groundwater potential zones in the crystalline basement terrain of South-West Nigeria: An integrated GIS and remote sensing approach. Appl Water Sci 4, 19–38.

Federal Department of Agricultural L Resources (FDALR), 1990. Soil map of Nigeria.

FMWR, 2014. The project for the review and update of Nigeria national water resources master plan. Federal Ministry of Water Resources (FMWR)/, 4. Japan International Cooperation Agency (JICA).

Foster, S., Tuinhof, A., Garduño, H., 2006a. Groundwater development in sub-Saharan Africa. A strategic overview of key issues and major needs. Sustainable Groundwater Management, lessons from practice, Case profile collection (15).

Foster, S., Koundouri, P., Tuinhof, A., Kemper, K., Nanni, M., Garduno, H., 2006b. Groundwater dependent ecosystems: the challenge of balanced assessment and adequate conservation; Sustainable Groundwater Management- Concepts and Tools, GW.Mate Briefing Note Series15, Washington DC,USA. Geosoft, 1997. Producing high-quality maps efficiently. Geosoft Technical Note, Geosoft Inc, pp. 1–14.

Grauch, V.J.S., Bankey, V., 2003. Aeromagnetic interpretations for understing the hydrogeologic framework of the Southern Espanola basin, New Mexico; United States Geol. Surv. MS 964, Federal Center, Denver, Co, p. 80225 -0046.

Greenbaum, D., 1992. Remote Sensing techniques for hydrogeological mapping in semi-arid basement terrains. Brit. Geol. Surv. NERC Techn..

Hamid-Mosaku, A.I., 2014. Intelligent geospatial decision support system for Malaysian marine geospatial data infrastructure (Unpublished doctoral dissertation). Universiti Teknologi Malaysia, Johor Bahru, Johor, Malaysia.

Hamid-Mosaku, I.A., Mahmud, M.R., Mohd, M.S., 2016. An evaluation of marine geospatial data infrastructure (MGDI) by delphi-analytic hierarchy process (AHP) approach. Jurnal Teknologi 78, 57–68 6-12.

Hamid-Mosaku, A.I., Mahmud, M.R., Mohd, M.S., Balogun, A.L., Raheem, K.A., 2017. Fuzzy evaluation of Marine Geospatial Data Infrastructure (MGDI): MGDI decisions' criteria. J. Eng. Res., Lagos 22 (1), 23–37.

Hamid-Mosaku, I.A, Oguntade, O., Ifeanyi, V.I., Balogun, A., 2020. Evolving a comprehensive geomatics multi-criteria evaluation index model for optimal pipeline route selection. Struct. Infrastruct. Eng.

Haque, S., Kannaujiya, S., Taloor, A.K., Keshri, D., Bhunia, R.K., Champati-Ray, P.K., Chauhan, P., 2020. Identification of groundwater resource zone in the active tec-

tonic region of Himalaya through earth observatory techniques. Groundw. Sustain. Dev. 10. doi:10.1016/j.gsd.2020.100337.
Harris Geospatial, 2020. Maximum likelihood.
Hasmadi, M., Pakhriazad, H.Z., Shahrin, M.F., 2009. Evaluating supervised and unsupervised techniques for land cover mapping using remote sensing data. Geogr. Malays. J. Soc. Space 5 (1), 1–10 2009.
Hoffmann, J., Sander, P., 2007. Remote Sensing and GIS in hydrogeology. Hydrogeol. J. 15 (1), 1–3.
Hubbard, B.E., Mack, T.J., Thompson, A.L., 2012. Lineament analysis of mineral areas of interest in Afghanistan. Open-File Report 2012–1048 USGS Afghanistan Project Product No. 233.
Huang, X., Weng, C., Lu, Q., Feng, T., Zhang, L., 2015. Automatic labelling and selection of training samples for high-resolution remote sensing image classification over urban areas. Remote Sens (Basel) 7 (2015), 16024–16044. doi:10.3390/rs71215819.
Ibraheem, M.I., Haggag, M., Tezkan, B., 2019. Edge detectors as structural imaging tools using aeromagnetic data: A case study of Sohag area, Egypt. Geosciences 9 (211), 1–13.
IGRAC, 2018. Adapting to climate change in the SADC region through water security – A focus on groundwater. International Groundwater Resources Assessment Centre (IGRAC), 1st SADC Groundwater Conference, South Africa.
Ishola, K.S, Akerele, P.O., Folarin, O., Adeoti, L., Adegbola, R.B., Adeogun, O.Y., 2020. Application of aeromagnetic data to map subsurface structural features in Ewekoro. Southwestern Nigeria., Model. Earth Syst. Environ. 2, 1171.
ISRIC, 1994. Lecture notes on the major soils of the world; World Soil Resources Reports, Food and Agriculture Organization. International Soil Reference and Information Centre (ISRIC).
Ishola, K.S., Nawawi, M.N.M., Abdullah, K., 2014. Combining multiple electrode arrays for two-dimensional electrical resistivity imaging using the unsupervised classification technique. Pure Appl. Geophys. 172, 1615–1642. doi:10.1007/s00024-014-1007-4, doi:.
Jasrotia, A.S., Bhagat, B.D., Kumar, A., Kumar, R., 2013. Remote Sensing and GIS approach for delineation of groundwater potential and groundwater quality zones of Western Doon Valley, Uttarakh. India. J. Indian Soc Remote Sens. 41 (2), 365–377. doi:10.1007/s12524-012-0220-9.
Jasrotia, A.S., Kumar, A., Singh, R., 2016. Integrated remote sensing and GIS approach for delineation of groundwater potential zones using aquifer parameters in Devak Rui watershed of Jammu Kashmir. India. Arab J Geosci. 9, 304. doi:10.1007/s12517-016-2326-9.
Jasrotia, A.S., Kumar, R., Taloor, A.K., Saraf, A.K., 2019. Artificial recharge to groundwater using geospatial and groundwater modelling techniques in Northwestern Himalaya. India. Arab J. of Geosci. 12, 774. doi:10.1007/s12517-019-4855-5.
Jesiya, N.P., Gopinath, G., 2019. A customized fuzzy AHP - GIS based DRASTIC-L model for intrinsic groundwater vulnerability assessment of urban /peri-urban phreatic aquifer clusters. Groundw. Sustain. Dev. 8, 654–666.
Jha, M.K., Chowdhury, A., Chowdary, V.M., Peiffer, S., 2007. Groundwater management and development by integrated remote sensing and GIS: Prospects and Constraints. Water Resour Manage 21, 427–467.
Jimoh, H.I., 1997. In: Predicting the factors of soil loss on different surfaces in Ilorin, Nigeria, 1. YOLDE, pp. 8–14.
Jimoh, H.I., 2011. Managing l use to control soil erosion problems in a part of Kwara State of Nigeria. J. Geogr. Reg. Plan. 4 (1), 36–41.
Kalhor, K., Ghasemizadeh, R., Rajic, L., Alshawabkeh, A., 2019. Assessment of groundwater quality and remediation in karst aquifers. Groundw. Sustain. Dev. 8, 104–121.
Karunakalage, A., Sarkar, T., Kannaujiya, S., Chauhan, P., Pranjal, P., Taloor, A.K., Kumar, S., 2021. The appraisal of groundwater storage dwindling effect, by applying high resolution downscaling GRACE data around Mehsana district, Gujarat, India. Groundw. Sustain. Dev. 13. doi.org/10.1016/j.gsd.2021.100559.
Kearey, P., Brooks, M., 1991. An introduction to geophysical exploration. Oxford Publishing House, Blackwell Scientific.
Khan, A., Govil, H., Taloor, A.K., Kumar, G., 2020. Identification of artificial groundwater recharge sites in parts of Yamuna River Basin, India based on Remote Sensing and Geographical Information System. Groundw. Sustain. Dev. 11. doi:10.1016/j.gsd.2020.100415.
Kumar, T.S., Mahendra, R.S., Nayak, Shailesh, Radhakrishnan, K., Sahu, K.C., 2010. Coastal vulnerability assessment for Orissa State, east coast of India. Journal of Coastal Research 26 (3), 523–534. doi:10.2112/09-1186.1.
Lawal, T.O., Sunday, J.A., Fawole, O., 2012. Impact of VES in delineation of groundwater distribution and exploration in hard rock terrain. Int. J. Adv. Phys. 4 (1), 30–35.
Lee, M.C., 2007. A method of performance evaluation by using the analytic network process and balanced score card. In: International Conference on Convergence Information Technology, pp. 235–240.
Levy, J., Xu, Y., 2011. Review: groundwater management and groundwater/surface-water interaction in the context of South African water policy. Hydrogeol. J. 20, 205–226.
Li, P., Qian, H., 2018. Water resources research to support a sustainable China. Int. J. Water Resour. Dev. 34 (3), 327–336.
Lillesand, T.M., Kiefer, R.W., 2010. Remote Sensing Image Interpretation, 4th ed. Wiley, New York 2000.
MacDonald, A.M., Davies, J., Calow, R.C., 2008. African hydrogeology and rural water supply. Applied Groundwater Studies in Africa 137–158.
Machiwal, L.D., Jha, M.K., 2014. Characterizing rainfall-groundwater dynamics in a hard-rock aquifer system using time series, geographic information system and geostatistical modelling. Hydrol. Process. 28, 2824–2843.
Madan, K.J, Chowdary, V.M., Chowdhury, A., 2010. Groundwater assessment in Salboni block, West Bengal (India) using remote sensing, GIS, and multi-criteria decision analysis techniques. Hydrogeol. J. 18 (7), 1713–1728.
Majumder, M., 2015. Multi-Criteria Decision Making: – Impact of urbanization on water shortage in the face of climatic aberrations; SpringerBriefs in Water Sci. Technol.
Magesh, N.S., Chrasekar, N., Soundranayagam, J.P., 2012. Delineation of groundwater potential zones in Theni District, Tamil Nadu, using remote sensing, GIS, and MIF techniques. Geosci. Front. 3 (2), 189–196.
Margat, J., Gun, V., 2013. Groundwater around the world: A Geographic Synopsis. CRC Press, Balkema Books, Taylor & Francis Group Leiden ISBN: 13:978-0-203-77214-0.
MMSD, 2017. Nigeria's mining and metal sector: Investment promotion brochure. Department of Planning, Research and Statistics, Ministry of Mines & Steel.
Mogaji, K.A., Aboyeji, O.S., Omosuyi, G.O., 2011. Mapping of lineaments for groundwater targeting in the basement complex region of Ondo State, Nigeria using remote sensing and GIS techniques. Int. J. Water Res. Environ. Eng 3 (7), 150–160.
Mogaji, K.A., 2016. Combining geophysical techniques and multi-criteria GIS-based application modelling: approach for groundwater potential assessment in southwestern Nigeria. Environ. Earth Sci. 75, 1181. doi:10.1007/s12665-016-5897.
Muthamilsevan, A., Srimadhi, K., Nhini, R., Pavithra, P., Balamuragan, T., Vasuki, V., 2017. Spatial confirmation of major lineament and groundwater exploration using ground magnetic method near Mecheri village, Salem District of Tamil Nadu, India. J. Geol. Geophys. 6 (1).
Mazac, O., Kelly, W.E., La, I., 1987. Surface geoelectrics for groundwater pollution protection studies. J.Hydrol 93 (3/4), 277–294.
Ndikilar, C.E., Idi, B.Y., Terhemba, B.S., Idowu, I.I., Abdullahi, S.S., 2019. Applications of aeromagnetic and electrical resistivity data for mapping spatial distribution of groundwater potentials of Dutse, Jigawa State, Nigeria. Mod. Appl. Sci. 13 (2), 11–20.
Nelson, H.D, Huffman, L.H, Fu, R., Harris, E.L., 2005. Genetic risk assessment and BRCA mutation testing for breast ovarian cancer susceptibility: systematic evidence reviews for the U.S. Preventive Services Task Force. Ann Intern Med 143, 362–379.
Nguyen, P., Shearer, E.J., Tran, H., Ombadi, M., Hayatbini, N., Palacios, T., Huynh, P., Braithwaite, D., Updegraff, G., Hsu, K., Kuligowski, B., Logan, W.S., Sorooshian, S., 2019. The CHRS data portal, an easily accessible public repository for PERSIANN global satellite precipitation data. Sci. Data 6 (1), 1–10.
Nigeria Geological Survey Agency (NGSA), 2010. Aeromagnetic data of Ilorin Sheet 223.
Nigeria Meteorological Agency (NiMet), 2010. Climate parameters of Ilorin for 30 years span.
Nwachokor, M.A., Uzu, F.O., 2008. Updated classification of some soil series in South-Western Nigeria. J. Agron. 7 (1), 76–81.
Nwankwo, L.I., 2002. Unpublished M.Sc. Thesis. University of Ilorin.
Nwankwo, L.I., 2011. 2D resistivity survey for groundwater exploration in a hard rock terrain: A case of MAGDAS observatory UNILORIN, Nigeria. Asian J. Earth Sci. 4 (1), 46–53.
Nwilo, P.C., Okolie, C.J., Onyegbula, J.C., Abolaji, O.E., Orji, M.J., Daramola, O.E., Arungwa, I.D., 2020. Vertical accuracy assessment of 20-metre SPOT DEM using ground control points from Lagos and FCT. Nigeria. J. Eng. Res. 25 (2), 153–164. http://jer.unilag.edu.ng/index.php/jer/article/view/997.
Nse, O.U., Okolie, C.J., Nse, V.O., 2020. Dynamics of land cover, land surface temperature and NDVI in Uyo capital city. Nigeria., Sci.Afri doi:10.1016/j.sciaf.2020.e00599.
Okpoli, C.C., Oladunjoye, M.A., 2017. Precambrian basement architecture and lineaments mapping of Ado-Ekiti region using aeromagnetic dataset. Geosci. Res. 2 (1).
Okunlola, O.A., 2012. Geoscience awareness in Nigeria – A preliminary study. J. Geosci. Educ. 60, 220–227 1089-9995/2012/60(3)/220/8.
Olasehinde, P.I., 1984. Unpublished M.Sc. Thesis. University of Ilorin.
Olasehinde, P.I., Raji, W.O., 2007. Geophysical studies of fractures of basement rocks at University of Ilorin, Southwestern Nigeria: Application to Groundwater Exploration. Water Resour 17, 3–10.
Olawepo, A.O., Fatoyinbo, A.A., Ali, I., Lawal, T.O., 2013. Evaluation of groundwater potential and subsurface lithologies in UNILORIN quarters using resistivity method. Afr. Rev. Phys. 8, 323–330.
Omeje, M., Husin, W., Noorddin, I., Oha, I.A., Onwuka, O.S., Soheil, S., 2014. Integrated geoelectrical and structural studies for groundwater investigation in parts of Abuja. North-central Nigera. Near Surf. Geophys. 12, 515–521. doi:10.3997/1873-0604-2014007.
Otukei, J.R., Blaschke, T., 2010. Land cover change assessment using decision trees, support vector machines and maximum likelihood classification algorithms. Int. J. Appl. Earth Obs. Geoinf. 12 (1), S27–S31. doi:10.1016/j.jag.2009.11.002, 2010Supplement.
Oyawoye, M.O., 1972. The basement complex of Nigeria. In: Dessauvagie, T.F.J., Whiteman, A.J. (Eds.), African Geology. University Press Ibadan., pp. 66–99.
Ozebo, V.C., Ogunkoya, C.O., Layade, G.O., Makinde, V., Bisilimi, A.L., 2017. Evaluation of aeromagnetic data of Ilesha area of Oyo state Nigeria using analytical signal (ASM) and local wavenumber (LWN). J.Appl.Sci.Environ.Manage 21 (6), 1157–1161.
Paine, J.W., 1986. A comparison of methods for approximating the vertical gradient of one-dimensional magnetic field data. Geophysics 51 (9), 1725–1735.
Prasad, R.K., Mondal, N.C., Banerjee, P., Nakumar, M.V., Singh, V.S., 2008. Deciphering

potential groundwater zone in hardrock through the application of GIS. Environ Geol 55, 467–475.
Raji, W.O., Bale, R.B., 2008. The Geology and geophysical Studies of a gravel deposit in University of Ilorin, SW-Nigeria. Continental J. Earth Science 3, 40–46.
Rahaman, M.A., 1988. Recent advances in the study of the Basement Complex of Nigeria. Precambrian Geology of Nigeria. Geological Survey of Nigeria Publication 11–43.
Ranganai, R.T., Ebinger, C.J., 2008. Aeromagnetic and Landsat TM structural interpretation for identifying regional groundwater exploration targets, South-central Zimbabwe Craton. J. Appl. Geophys. 65, 73–83.
Rao, N.S., Chaudhary, M., 2019. Hydrogeochemical processes regulating the spatial distribution of groundwater contamination, using pollution index of groundwater (*PIG*) and hierarchical cluster analysis (HCA): A case study. Groundw. Sustain. Dev. 9, 100238.
Reisi, M., Afzali, A., Aye, L., 2018. Applications of analytical hierarchy process (AHP) and analytical network process (ANP) for industrial site selections in Isfahan. Iran. Environ. Earth Sci. 77 (14), 537.
Reeves, C.V., 1989. In: Aeromagnetic interpretation and rock magnetism, 7. First Break, pp. 275–286.
Roest, W.R., Verhoef, J., Pilkington, M., 1992. Magnetic interpretation using the 3-D analytic signal. Geophysics 57, 116–125.
Saaty, T.L., 1980. The analytical hierarchy process, planning, priority. Resource allocation. RWS publications, USA.
Saaty, T.L., 1988. What is the analytic hierarchy process? In: In mathematical models for decision support. Springer, Berlin, Heidelberg, pp. 109–121.
Saaty, T.L., Kearns, K.P., 1985. Analytical Planning: The Organization of Systems. Pergamon Press, Oxford.
Sander, P., 2007. Lineaments in groundwater exploration: A review of applications and limitations. Hydrogeol. J. 15, 71–74.
Sarkar, T., Kannaujiya, S., Taloor, A.K., Prashant Kumar Champati-Ray, P.K., Chauhan, P., 2020. Integrated study of GRACE data and derived interannual groundwater storage variability over water stressed Indian regions. Groundw. Sustain. Dev. 10. doi:10.1016/j.gsd.2020.100376.
Shiklomanov, I.A., Gleick, P.H., 1993. World freshwater resources. Water in Crisis, New York.
Skiba, P., Gabriel, G., Krawczyk, C.M., Konig, M., Bucker, C., Rolf, C., 2016. On the use of small amplitude magnetic anomalies for the Improvement of geological models: Case studies from Northern Germany. Z. Dt. Ges. Geowiss (German J.Geol) 167 (2/3), 131–148.
Silwal, C.B., Pathak, D., 2018. In: Review on practices and state of the art methods on delineation of groundwater potential using GIS and remote sensing, 20/21. Bulletin of Department of Geology, Tribhuvan University, Kathmu, Nepal, pp. 7–20.
Srivastava, S., Agarwal, B.N.P., 2010. Inversion of the amplitude of the two-dimensional analytic signal of the magnetic anomaly by the particle swarm optimization technique. Geophys. J.Int 182, 652–662.
Swetha, T.V., Gopinath, G., Thrivikramji, K.P., Jesiya, N.P., 2017. Geospatial and MCDM tool mix for identification of potential groundwater prospects in a tropical river basin. Kerala. Environ Earth Sci 76, 428. doi:10.1007/s12665-017-6749-8.
Todd, D.K., 1980. Groundwater Hydrology. J. Wiley & Sons, New York.
Tóth, J., 1999. Groundwater as a geologic agent: An overview of the causes, processes, and manifestations. Hydrogeology Journal 7, 1–14.
United State Geological Survey (USGS), 2013. Lsat 8 OLI/TIRS satellite imagery - Path 190 Row 54.
United States Geological Survey (USGS), 2020. Earth Resources Observation Science (EROS) Center Science Processing Architecture (ESPA) on DEM interface user guide Release 3.0.0. Version 4.0.
WMO, 2012. Technical material for water resources assessment: Technical report series No.2. World Meteorological Organization, 7 bis avenue de la paix, Geneva 2, Switzerl.
Zhang, X., Li, X., Feng, Y., Liu, Z., 2015. The use of ROC and AUC in the validation of objective image fusion evaluation metrics. Signal process 115, 38–48.
Zhou, W., 2018. Aeromagnetic survey. In: Bobrowsky, P.T., Marker, B. (Eds.), Encyclopedia of Engineering Geology. Encycl. Earth Sci. Series. Springer, Cham.